ACS APPLIED ELECTRONIC MATERIALS

Subscriber access provided by Uppsala universitetsbibliotek

Article

External Quantum Efficiency of 6.5% at 300nm emission and 4.7% at 310nm emission on bare-wafer of AlGaN-based UVB LEDs

Muhammad Ajmal Khan, Yuri Itokazu, Noritoshi Maeda,
Masafumi Jo, Yoichi Yamada, and Hideki Hirayama

ACS Appl. Electron. Mater., **Just Accepted Manuscript** • DOI: 10.1021/acsaelm.0c00172 • Publication Date (Web): 06 Jun 2020

Downloaded from pubs.acs.org on June 8, 2020

Just Accepted

"Just Accepted" manuscripts have been peer-reviewed and accepted for publication. They are posted online prior to technical editing, formatting for publication and author proofing. The American Chemical Society provides "Just Accepted" as a service to the research community to expedite the dissemination of scientific material as soon as possible after acceptance. "Just Accepted" manuscripts appear in full in PDF format accompanied by an HTML abstract. "Just Accepted" manuscripts have been fully peer reviewed, but should not be considered the official version of record. They are citable by the Digital Object Identifier (DOI®). "Just Accepted" is an optional service offered to authors. Therefore, the "Just Accepted" Web site may not include all articles that will be published in the journal. After a manuscript is technically edited and formatted, it will be removed from the "Just Accepted" Web site and published as an ASAP article. Note that technical editing may introduce minor changes to the manuscript text and/or graphics which could affect content, and all legal disclaimers and ethical guidelines that apply to the journal pertain. ACS cannot be held responsible for errors or consequences arising from the use of information contained in these "Just Accepted" manuscripts.

is published by the American Chemical Society. 1155 Sixteenth Street N.W., Washington, DC 20036
Published by American Chemical Society. Copyright © American Chemical Society. However, no copyright claim is made to original U.S. Government works, or works produced by employees of any Commonwealth realm Crown government in the course of their duties.

1
2
3
4
5
6
7

External Quantum Efficiency of 6.5% at 300nm emission and 4.7% at 310nm emission on bare-wafer of AlGaN-based UVB LEDs

M. Ajmal Khan,[1,2,] Yuri Itokazu,[1] Noritoshi Maeda,[1] Masafumi Jo,[1] Yoichi Yamada,[3] Hideki Hirayama[1,2]*
[1]RIKEN Cluster for Pioneering Research (CPR), 2-1 Hirosawa, Wako, Saitama 351-0198, Japan
[2]RIKEN Center for Advanced Photonics (RAP), 2-1 Hirosawa, Wako, Saitama 351-0198, Japan
[3]Yamaguchi University, 2-16-1 Tokiwadai, Ube Yamaguchi 755-8611, Japan
**Corresponding author: muhammad.khan@riken.jp*

Abstract: By the Minamata Convention on Mercury, regulation on Mercury use will be stricter from this year of 2020 and safe AlGaN-based ultraviolet (UV) light sources are urgently needed for killing of SARS-CoV-2 (corona virus). AlGaN-based ultraviolet‐B (UVB) light‐emitting diodes (LEDs) and UVB laser diodes (LDs) have the potential to replace toxic mercury UV-Lamps. Previously, the internal-quantum-efficiency (η_{int}) were enhanced from 47% to 54% in AlGaN UVB multi-quantum-well (MQWs). However, some non-linear behavior in both light output power (L) and external-quantum-efficiency (η_{ext}) in the 310nm-band UVB LEDs were observed and later on such nonlinearities were overcome by reducing the thicknesses of quantum-well-barriers (T_{QWB}) in MQWs. After relaxing to the n-AlGaN electron injection layer (EIL) up to 50% underneath the MQWs and using highly reflective Ni/Al p-electrode, the L and η_{ext}, respectively, of 310nm-band UVB LED were greatly improved from 12 mW and 2.3% to a record value of 29 mW and 4.7%. Similarly, for 294nm-band UVB LED, the η_{ext} and L, respectively, were also remarkably improved up to 6.5% and 32 mW at RT on bare-wafer condition, using better carrier confinement scheme in the MQWs as well as using moderately Mg-doped p-type multi-quantum-barrier electron-blocking-layer (p-MQB EBL). Moderately doped p-MQB EBL was aimed for better hole transport to enhance the hole injection toward the MQWs as well as to block the high energy electron from overshooting. Possible explanations and recommendations for the improvements in the performances of 294-310nm UVB LEDs are broadly discussed. Most importantly, such controllable multi UVB-wavelength emitters may extend nitride‐based LEDs to previously inaccessible areas, for example, electrically pumped AlGaN-based UVB LDs.

Keywords: LP-MOVPE, AlGaN, MQWs, UVB LED, AlN template, total-TDDs, IQE, EQE, light power, carrier confinement, p-AlGaN hole injection layer, polarized p-AlGaN contact layer

1
2
3
4
5
6
7
8
9
10
11
12
13
14
15
16
17
18
19
20
21
22
23
24
25
26
27
28
29
30
31
32
33
34
35
36
37
38
39
40
41
42
43
44
45
46
47
48
49
50
51
52
53
54
55
56
57
58
59
60

1. Introduction

Eco-friendly materials for low cost, and efficient deep ultraviolet (DUV), ultraviolet-B (UVB) light-emitting diodes (LEDs) and UVB laser diodes (LDs) with high power have been of great importance for both medical and agricultural applications [1-8]. Among such materials, we have been focused on semiconducting aluminum gallium nitride (AlGaN) – based UVB LEDs and UVB LDs grown on AlN template [7-9]. Due to the global corona pandemic, urgent efforts are needed to combat the growth and expansion of SARS-CoV-2, which is the virus that causes COVID-19 infections, and UV light can kill the novel COVID-19 [1]. Furthermore, safe AlGaN-based UVB LEDs devices are strongly needed for both medical and agricultural applications such as those in cancer immunotherapy, vulgaris treatment (310nm) [2-4], plant growth under UVB lightning (310nm), prevention of plant diseases (294nm) [4,10], the production of vitamin D_3 in the human body (294nm) [4-6,11], and production of phytochemicals in the green leaves of vegetable (310nm) [8,12]. UVA is not suitable for the treatment of psoriasis [4,8,13]. Narrow-band (NB)-UVB at 310nm emission therapy was found to be more effective than the Broadband (BB)-UVB (280nm-320nm) therapy in the treatment of psoriasis and atopic dermatitis [8,14-15]. Therefore, NB-UVB phototherapy (instead of BB-UVB) at 310 nm emission are used for cancer therapy as well as for skin cure therapy [14-20]. NB-UVB light sources are recommended for the treatment of psoriasis by USA and some other countries too [14,21-22]. Ramnemark et al. investigated the distributions of vitamin D_3 in a human population living above 638 N^0 (Europe) and it was found that 23.1% of men and 17.1% of women had insufficient levels of vitamin D_3 [11]. It was also reported that 293nm-band UVB LEDs are more efficient than sunlight for producing vitamin D_3 in the human body [4-5], as well as in animal body too. UVB light sources in the spectral range of 280-290nm were found effective in suppression of the tomato mosaic virus (ToMV) in tomato plants [10]. Eco-friendly AlGaN-based DUV and UVB LED light sources has many advantages to be used for suppression of virus in plants, in hospital, in care center as well as in quarantine center, when compared to some pesticides or germicide disinfectants [8]. Comprehensive review studies about the use of UVB light sources for both medical and agricultural applications are discussed elsewhere [4, 8, 23-25].

Based on this comparative review study of UVB light sources for both medical and agricultural applications, two important UVB-wavelength emission at 294 nm and 310 nm were carefully chosen for the improvement of quality of life (QOL) [4, 8, 25]. AlGaN materials are promising for the development of NB-UVB LEDs and also for the fabrication of some other electronic and optical devices including UVB LDs [8]. The bandgap of $Al_{1-x}Ga_xN$ can be controlled as a function of Al composition (x) between 6.2 eV (AlN) and 3.4 eV (GaN), which can be tuned for the desired wavelength NB-emission from UVA, UVB and UVC LEDs [7-9, 23]. AlGaN materials are more advantageous over mercury (Hg) for making UVB LED light sources as: (i) high internal-quantum-efficiency (η_{int}) from the AlGaN-based MQWs at NB-UVB emission is possible, (ii) both p- and n-type semiconductors in the wide-bandgap spectral region can be grown to complete the p-n junction diode, (ii) AlGaN is mechanically hard material, and therefore the UV devices might be having longer life, and (iv) AlGaN materials are transparent for UV-light and also free from harmful or toxic materials, i.e. Arsenic (As), Mercury (Hg) and Lead (Pb). The possibility of a NB electroluminescence (EL) emission from the AlGaN-MQW is quite high, when compared to Hg-UV Lamp [7-9, 25]. Thanks to the Manasevit et. al. [23] successfully grown GaN and AlN in 1971 for the first time, by using metal-organic chemical vapor deposition (MOCVD). AlGaN crystal can be grown on AlN template on c-sapphire substrate for UV emitters [3-4,7-9,26-27]. However, the c-sapphire substrate is electrically insulating and due the large bandgap energy of sapphire (8.8 eV), it is fully transparent for the entire spectral range of UVA, UVB, and UVC [8]. In order, to enable electron injection smoothly and current-spreading uniformly to MQWs, therefore well optimized Si-doped n-AlGaN buffer layer (BL) and n-AlGaN electron injection layer (EIL)

1
2
3
4
5
6
7
8
9
10
11
12
13
14
15
16
17
18
19
20
21
22
23
24
25
26
27
28
29
30
31
32
33
34
35
36
37
38
39
40
41
42
43
44
45
46
47
48
49
50
51
52
53
54
55
56
57
58
59
60

were subsequently deposited [3-4,24-26] on the AlN template grown on C-Sapphire substrate [7-8]. High efficiency AlGaN-based DUV and UVC emitters were successfully grown using n-AlGaN BL on the AlN template [7-9]. However, high performance of the AlGaN-based UVB LEDs grown on AlN template are still exceedingly rare [3-4, 24-31].

Truly little work has been done so far on the subject of high efficiency (290-310nm)-band AlGaN UVB LEDs grown on AlN template on c-sapphire substrate [4,8]. Kim et al. demonstrated (290-305nm)-band AlGaN UVB LEDs grown on an AlN template, where a maximum light output power (L) of 1.8 mW at 290nm emission and 2.7 mW at 305nm emission were reported [27]. Similarly, AlGaN-based 302nm-band UVB LEDs grown on AlN templates were reported by TU Berlin [28]. Also, AlGaN (InAlGaN)-based UVB LEDs at 310nm emission was grown on an AlN template and the devices performances were demonstrated [30]. The maximum L were restricted to 1.6 mW at 60 mA [29], and to 18 mW at 500 mA [30] of the UVB LEDs. The maximum external-quantum-efficiency (η_{ext}) were also restricted to the range of 0.9-2.3% at 310nm emission [3,25,31]. The performances of the (290-310nm)-band UVB LEDs grown on AlN templates are still very low, due to the existence of high total threading-dislocation densities (total-TDDs) and point defects in n-AlGaN EIL underneath the MQWs and also due to the unavailability of high hole injection from the p-AlGaN hole source layer (HSL) to the MQWs [3-4, 24-25]. The annihilation and suppression of total-TDDs in our home-grown n-AlGaN EIL underneath the MQWs for the applications of UVB LEDs will be discussed and elaborated in this paper. In addition, some brief discussion about TDDs, 3D growth modus, phase separation or kinetic separation as well as the existence of macro-steps in the n-AlGaN EIL and MQWs will be provided in subsection 3.1. The crystalline quality of Si-doped n-AlGaN EIL underneath the MQWs for both UVA and UVB emitters were greatly improved [4, 26]. In addition to that, high relative transmittance ≥ 90% through transparent p-AlGaN hole injection layer (HIL) including p-AlGaN contact layer [3-4, 24-25] for the applications of (290-320nm)-band UVB LEDs were realized. However, the problem of high total-TDDs in the n-AlGaN EIL underneath MQWs (causes low η_{int}), nonlinearity in the I-L and I-η_{ext} at low drive current were the remaining issues in our previous work of ref [25]. Such nonlinearities due to current injection were resolved by using both optimized undoped (ud)-AlGaN final barrier (FB) as well as using optimized thickness of quantum-well-barriers (QWBs) in the MQWs [3].

In this paper, progress on AlGaN-based UVB LEDs at 294-310nm emission wavelengths will be briefly reviewed and two improved results of UVB LEDs are discussed, as shown in Figs. 1(a)-(c). In particular the route toward the engineering of high quality of n-AlGaN EIL underneath the MQWs will be discussed in the context of η_{int}. Furthermore, the influence of p-type electrodes as well as varying number of n-AlGaN BLs on the recovery of nonlinear behavior in L and η_{ext} are briefly discussed. Previously, the influence of the partially relaxed (relaxation ratio ~ 50%) n-AlGaN EIL on the device performances of (294-310nm)-band UVB LEDs were not studied [3, 25]. The influence of both thickness of ud-AlGaN FB (T_{FB}) and Al-alloy contents in the ud-AlGaN FB on the hole transport was studied and the devices performances were quite improved [4]. Furthermore, the improved design of ud-AlGaN FB were found to be promising for the blocking of Mg-atoms diffusion toward MQWs from multi-quantum-barrier electron-blocking-layer (MQB EBL) [4,24-25]. However, the carrier confinement issue in the MQWs of our previous 294nm-band UVB LEDs was not considered [3-4, 24-25]. Also, the influence of 4µm-thick n-AlGaN BL on the partial relaxation of the n-AlGaN EIL underneath the MQWs for 310nm-band UVB LED was not studied.

Briefly speaking, in this paper the influence of the 3.4 µm-thick n-AlGaN BL and partially relaxed (relaxation ratio ~ 50%) n-AlGaN EIL on the device performance of 310nm-band UVB LED was our main objective. The influence of large and small size of highly reflective (Ni/Al) p-electrode on the device performances as well as on the droop behavior in

ACS Paragon Plus Environment

1
2
3
4
5
6
7

the η_{ext} of (294-310nm)-band UVB LED were also considered. For 294nm-band UVB LED, the carrier confinement issue in the MQWs was further investigated. Especially the Al-alloy differences between QWBs and quantum-wells (QWs) were enhanced in the context of carrier confinement in the MQWs. For hole intraband tunneling (HIT) to toward the MQWs, one new design of moderately Mg-doped p-type multi-quantum-barrier electron-blocking-layer (p-MQB EBL) was introduced to 294nm-band UVB LED. Finally, brief roadmap for pressing challenges in the AlGaN-based UVB LEDs, namely the reduction of total-TDDs in the n-AlGaN EIL underneath the MQWs (for the enhancement of η_{int}), activation of the Mg-atoms in the p-AlGaN layers (high carrier injections toward the MQWs by polarizability in the p-AlGaN hole-injection-layer (HIL) and reduction of operating voltages by using Flip-Chip technology (FC) were also discussed. Last but not the least, how to improve the light extraction efficiency (η_{lee}) beyond 20% in the current UVB LEDs, will be briefly discussed.

2. Experimental Methods and Techniques

Previously, several type of UVB LED devices were grown on AlN template on sapphire substrate at emission-band of 310 nm and 295nm [4, 24-25], using low-pressure metalorganic vapor phase epitaxy (LP-MOVPE). All samples of AlGaN-based UVB LED devices were grown on AlN template on C-plan Sapphire substrate, using ammonia (NH_3) pulsed-flow multilayer (ML) crystal growth technique in LP-MOVPE [7-8, 32]. Based on sample-N/sample-P [3], and sample-A [4], two improved UVB LED devices sample-HK01 (at 310 nm emission) as well as sample-HK02 (at 300 nm emission) were grown, shown in Figs. 1(a)-(b). More handsome information about the pre-growth process (thermal cleaning), and types of gas precursors used for the crystal growth of p-AlGaN and n-AlGaN stacking layers have been discussed elsewhere in Ref [4, 24-25].

Briefly speaking, using good crystalline quality (total-TDDs ~5×10^{8} cm^{-2}) of 4μm-thick AlN template [7-8, 32], two improved samples were grown in a LP-MOVPE reactor. First, the sample-HK01 (for 310nm-band emission UVB LED) was grown, shown in Fig. 1(a). An approximately 3.4 μm-thick Si-doped n-$Al_{0.60}Ga_{0.40}N$ BL and then relatively Ga-rich 200nm-thick Si-doped n-$Al_{0.44}Ga_{0.56}N$ EIL were grown (sample HK01) on AlN template. The Si concentrations of approximately 7×10^{18} cm^{-3} were kept in both the n-AlGaN BLs and n-AlGaN EIL layers (electron source layer). Next, three-fold structure of $Al_{0.30}Ga_{0.70}N$ (3-4nm) quantum-well (QW) / $Al_{0.40}Ga_{0.60}N$ (10 nm) QWB were grown on the overlayer of n-AlGaN EIL as a MQWs region for 310nm-band UVB LED. Next, 12nm-thick ud-$Al_{0.44}Ga_{0.56}N$ FB was grown for the dual purposes of blocking of Mg-atoms diffusion toward MQWs and also for confining of low energy electron to MQWs of p-n junction diode. Subsequently, a twofold moderately Mg-doped (EBL-I and EBL-II) p-$Al_{0.60}Ga_{0.40}N$ blocking (20nm)/p-$Al_{0.30}Ga_{0.70}N$ valley (10nm) structures were grown as a p-MQB EBL to suppress the overshooting of high energy electron toward the p-AlGaN HIL and at the same time to facilitate the efficient hole transport from the p-AlGaN HIL to MQWs. Finally, a 130nm-thick Mg-doped p-$Al_{0.47}Ga_{0.53}N$ HIL and 20nm-thick p^{+}-AlGaN contact layer, respectively, were grown on p-MQB EBL. The Mg concentrations of 6×10^{19} cm^{-3} were set in the p-AlGaN HIL, as compared to the Si concentrations level of 7×10^{18} cm^{-3} in the n-AlGaN EIL of sample-HK01 (310nm-UVB LED). The details about the growth condition of sample-HK01 has been discussed elsewhere [3].

For 300nm-band UVB LED one improved structure (sample-HK02) was successfully grown, as shown in Fig. 1(b) and more detail about the layer by layer growth condition has been given in the table. 1. Previously, we used 48% Al-composition in the ud-AlGaN FB of sample-B [24-25], and later on, the Al-composition were increased up to 55% in the ud-AlGaN FB (sample-A) [4], of 294nm UVB LED, as shown in the Figs. 8(b)-(c). In sample-HK02 the Al-alloy difference between quantum-well-barrier (QWB) and quantum-well (QW) were increased from 15% (sample-A) [4], to 20% (this work) for better carrier confinement in the MQWs. In sample-HK02, an approximately 5-6nm thick ud-AlGaN FB

layer was also introduced in between the p-type multi-quantum-barrier electron-blocking-layer (p-MQB EBL) and MQWs for better hole transport as well as for suppression of Mg-diffusion toward the MQWs. In sample-HK02, the conventional MQB-EBL was replaced by a new design of moderately Mg-doped p-MQB EBL, as shown in Fig. 1(b) and (c). The Si-concentration level of approximately 6×10^{18} cm^{-3} were fixed in both the n-AlGaN BL and n-AlGaN EIL layers, respectively. By using high quality of 4μm-thick AlN template [7-8,32], a Si-doped n-$Al_{0.55}Ga_{0.45}N$ BL, and relatively Ga-rich Si-doped n-$Al_{0.47}Ga_{0.53}N$ EIL were grown, as shown in table. 1. Subsequently, threefold MQWs region of $Al_{0.30}Ga_{0.70}N$ QW/ $Al_{0.49}Ga_{0.51}N$ (QWB) as well as ud-$Al_{0.55}Ga_{0.45}N$ FB were grown on the n-AlGaN EIL. Subsequently, p-MQB EBL were grown on ud-AlGaN FB, where p-$Al_{0.16}Ga_{0.80}N$ Valley were sandwiched between p-$Al_{0.55}Ga_{0.45}N$ EBL-I, and p-$Al_{0.55}Ga_{0.45}N$ EBL-II, as shown in Fig. 1(b) and given in table. 1. Finally, Mg-doped p-$Al_{0.52}Ga_{0.48}N$ HIL and p-$Al_{0.52}Ga_{0.48}$ contact layer, respectively, were grown on the overlayer of p-MQB EBL structure, as shown in Fig. 1(b) and table. 1. The Mg-concentration of approximately 6×10^{19} cm^{-3} in the p-AlGaN HIL as well as approximately of 7×10^{19} cm^{-3} in the p-AlGaN contact layer were set in the sample-HK02. More details information about the growth conditions of sample-HK02 have been given in table. 1.

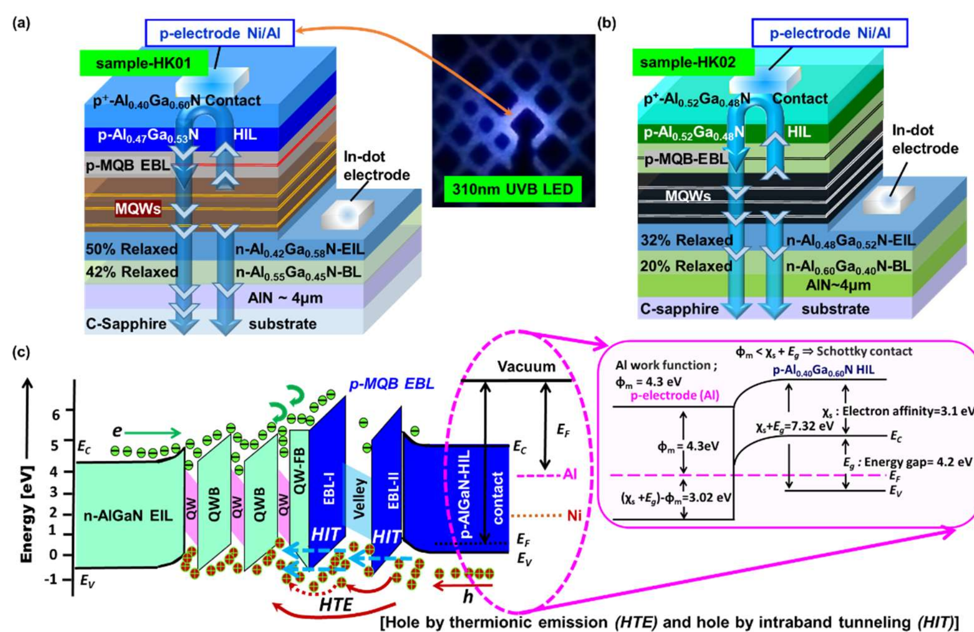

Fig. 1 (a) schematic view of 3.4 μm-thick n-AlGaN BL and 50% relaxed n-AlGaN EIL based 310nm-band UVB LEDs using a highly-reflective Ni/Al p-electrode, (b) schematic view of 1.7 μm-thick n-AlGaN BL and 30% relaxed n-AlGaN EIL based 294nm-band UVB LEDs (the real image of UVB LED with both In-dot n-electrode and Ni/Al p-electrode is shown in the inset), and (c) Estimated energy band diagram of typical AlGaN UVB LED with six distinct regions including the p-electrode (Ni/Al) contact structure (in this work).

Schematic view of the grown sample-HK02 (UVB LED) is shown in Figure. 1(b), which is not to scale and only for guidance. The estimated energy band diagram of the sample-HK02 has been shown in Fig. 1(c), where depiction of hole transport enhancement via p-MQB EBL has been shown. In order to improve the hole injection toward MQWs, to suppress Mg-diffusion from MQWs as well as to suppress the over shooting of low energy electrons toward the p-

Table. 1 crystal growth condition of AlGaN-based UVB LED (sample-HK02)

sample-HK02 (structure)	Growth Temp (°C)	Thickness (nm)	TMGa (sccm)	TMAl (sccm)	TESi (sccm)	Cp2Mg (sccm)	NH_3 (sccm)	Relaxation ratio (%)	Al-composition(%)
n-AlGan BL-1	1140	1700	4.0	20.0	0.1	0.0	2000	20	55
n-AlGaN EIL	〃	200	6.0	20.0	0.1	0.0	〃	32	47
3fold QW (MQWs)	〃	2-3	4.5	8.0	0.0	0.0	〃	32	30
3fold QWB (MQWs)	〃	8	5.0	20.0	0.02	0.0	〃	32	49
ud-AlGaN FB	〃	6	6.0	28.0	0.0	0.0	〃	--	55
EBL-I (p-MQB EBL)	〃	20	3.4	30.0	0.0	30	〃	--	55
Valley (p-MQB EBL)	〃	8	6.0	16.0	0.0	30	〃	--	16
EBL-II (p-MQB EBL)	〃	30	3.4	30.0	0.0	30	〃	--	55
p-AlGaN HIL	〃	130	5.4	20.0	0.0	70	〃	--	47
p-AlGaN contact	〃	20	5.4	20.0	0.0	80	〃	--	47

AlGaN HIL including p-AlGaN contact layer, we have recently proposed a very thin ud-AlGaN FB as well as moderately Mg-doped p-MQB EBL accompanied by a very thin Valley that has a smaller energy band gap for the UVB LED (sample-HK02), as shown in Fig. 1(c). The working device structure is shown in the estimated schematic view of energy band diagram with six distinct regions including the p-electrode (Ni/Al) contact layer of typical AlGaN UVB LED, shown in Fig. 1(c). The six distinct regions are; (1) the Si-doped n-type AlGaN EIL (electron injection layer) for lateral-type current spreading, (2) the active region (3fold-MQWs) for electron and hole pair confinement and for radiative recombination process, (3) the undoped (ud)-AlGaN FB, for hole tunneling, for suppression of Mg-atoms diffusion in to MQWs as well as for suppression of overshooting of low energy electron toward the p-AlGaN HIL side [4], (4) state of the art, moderately Mg-doped p-type MQB EBL (electron-blocking layer) for effective high energy electron blocking and supporting to the hole injection by thermionic emission (HTE) as well as hole by intraband tunneling (HIT) after the generation of 2D gas at the interfaces of the EBL-I, Valley, and EBL-II, shown in Fig. 1(c), (5) the highly transparent p-type p-AlGaN HIL including p-AlGaN contact layer [33], and (6) highly reflective Ni/Al p-electrode as contact layer with p-AlGaN contact. Owing to the large difference in the electron and hole transport behavior in III-V materials, the electrons can easily overshoot from the active (MQWs) toward the p-region of the UVB emitters. Hence, apart from the challenges facing by UVB LEDs and LDs, the efficiency droop at high current injection and poor hole injection toward the MQWs, leading to relatively poor radiative recombination and ultimately the devices performances of DUV LEDs and UVB LEDs were deteriorated [7-9, 24-25]. To overcome these issues the poor carrier transport from p-AlGaN HIL to MQWs via EBL is revisited. To enhance the intraband-tunneling-assisted hole injection (HIT), we have implemented a state-of-the-art p-MQB EBL with a very thin Valley (8nm). Valley has a smaller energy band gap than the EBL-I and EBL-II for the new design of UVB LED, as shown in the Fig. 1(c). As we know that the major hole transport in the conventional bulk p-EBL in the UVB LED, is mostly taking place via the thermionic emission, which is strongly dependent on the valence band offset and the hole concentration, as given by the following Eq. (1) as:

$$\emptyset_h = \Delta E_V - kT * \ln(p/N_v). \quad (1)$$

where, $\emptyset_h$: valence band barrier height, ΔE_V: valence band offset, k : Boltzmann constant, T: the carrier temperature, p: hole concentration, and N_V : effective density of states for holes. Therefore, it is highly desired to reduce valence band barrier height ($\emptyset_h$) by increasing the hole concentration "p". Thanks to the thin AlGaN layer (Valley) between EBL-I and EBL-II with a smaller energy bandgap, if inserted properly, the hole concentration can be increased

1
2
3
4
5
6
7
8
9
10
11
12
13
14
15
16
17
18
19
20
21
22
23
24
25
26
27
28
29
30
31
32
33
34
35
36
37
38
39
40
41
42
43
44
45
46
47
48
49
50
51
52
53
54
55
56
57
58
59
60

into the p-MQB EBL. More importantly, the Valley insertion layer should be close to the p-AlGaN HSL (hole source layer), as shown in Fig. 1(c). Once the Valley layer is reasonably thin, the holes can be injected into the Valley layer from p-AlGaN HIL by both the thermionic emission (HTE) and the intraband tunneling process (HIT) and then easily be transported to MQWs. It can be further explained that: by the polarization field effect, which is generated at the interfaces of EBL-I, -II and Valley (between Valley and quantum barrier) i.e. The electric field in a p-MQB EBL is obtained by subtracting the polarization of a Valley from that of a quantum barrier (QB: electron blocking layer) of p-MQB EBL [34], which can be express in the following Eq. (2) as:

$$\Delta P = P^{QB} - P^{Valley}. \qquad (2)$$

As a result of the polarization field effect, a high local hole concentration "p" can be obtained in the thin Valley, which helps in the decrease of the valence band barrier height $\emptyset_h$, for hole injection from the hole source layer (p-AlGaN HIL) toward the MQWs. This effect has been shown schematically in Fig. 1(c).

Furthermore, highly transparent p-AlGaN HIL including p-AlGaN contact layer and highly reflective p-electrode are quite necessary for the enhancement of the LEE (η_{lee}) desired by Eq (3). Rhodium (Rh) material as a p-electrode could be a good option to serve the purposes of both low operating voltage as well as high reflectivity, however Rh is quite expensive. Therefore, we opted for low cost and highly reflective Ni (1nm) /Al (200nm) based type p-electrode, as shown in Fig. 1(a)-(c). The electronic band arrangement between p-AlGaN contact layer and Ni/Al p-electrode has been shown in the inset of Fig. 1(c).

The crystal quality, Al-compositions and strain-relaxation ratio were investigated, using XRD measurement of rocking curves (XRCs) and reciprocal space mapping (RSM) for sample-HK01 and –HK02. Cross-section of high-angle annular dark field scanning-transmission-electron-microscopy (HAADF-STEM) and annular bright-field scanning-transmission-electron-microscopy (ABF-STEM) were performed for the evaluation of the total-TDDs. The Photoluminescence (PL) spectra were measured both at room temperature (RT) as well as at low temperature (LT). For UVB MQWs at 295nm emission [25], the excitation source for the standard IQE measurement was provided by second harmonic of a dye laser, pumped by a Xe–Cl excimer laser [35]. Secondary ion mass spectroscopy (SIMS) were performed to characterize the depth profiles of Mg-atoms in the moderately Mg-doped p-MQB EBL of UVB LED (sample-HK02). Highly reflective 1nm-thick Ni film followed by 200nm-thick Al (total reflectance ~ 84%) film were evaporated on the p-AlGaN contact layer in all samples, for the enhancement of η_{lee} as suggested by Eq. (3), shown in Figs. 1(a)-(c). In (Indium)-dot based n-type electrodes were deposited on all samples for quick check measurement, as shown in the schematic view of Fig. 1(a) and 1(b) and the same has been indicated in the real image of Fig. 9(b). The performances of all 310nm-band and 300nm-band UVB LED devices were evaluated at RT under both continues wave (CW)-operation as well as pulse-operation using p-type electrodes with different chip sizes on bare-wafer condition. The real images of chips with different sizes has been shown in the inset of Fig. 6(c) and 6(d). All the reported values of L in this work correspond to the total radiant flux from the UVB LEDs, which was calibrated for the accurate measurement of the luminous flux for the output power [24-25, 36-37]. By using the Si photodetector was set behind the test samples, the output power *(L)* was measured on bare-wafer under continuous wave (CW)-and pulse-operation at RT.

1
2
3
4
5
6
7
8
9
10
11
12
13
14
15
16
17
18
19
20
21
22
23
24
25
26
27
28
29
30
31
32
33
34
35
36
37
38
39
40
41
42
43
44
45
46
47
48
49
50
51
52
53
54
55
56
57
58
59
60

3. Results and Discussions

In this section, we provide in-depth discussion and explanation starting from the crystal growth characterization down to the optical as well as to electrical characterization of both UVB LEDs at 300nm as well as at 310nm emission, respectively. The merit of equation for UVB emitters can be express in Eq. (3). The maximum η_{ext} and maximum η_{int}, respectively, achieved so far from an AlGaN-based UVB LEDs at emission wavelength of 290-310nm in our lab at Riken are in the ranges of 47-54% and 2.3-5.6% [3-4, 24-25] and these values were found still very low as compared to the UVC LEDs [7-8, 38-41], to replace toxic Mercury UV-Lamps. The bottleneck of efficient UVB LED devices is to further increase the η_{ext} as:

$$\eta_{ext} = \eta_{int} \times \eta_{inj} \times \eta_{lee}, \qquad (3)$$

where η_{int} = internal-quantum-efficiency (IQE), which depends on the bulk total-TDDs, contaminations, point defects, interface states defect density both at the interface of n-AlGaN EIL and MQW, and choice of the substrate conditions [7-8]. Furthermore, thicknesses of the QWs and QWBs are the most important parameters to suppress the piezoelectricity as well as the uniform distribution of electron-hole (e-h) pairs in the MQWs. By this way, we can improve the IQE in the active region of the UVB LED devices. Similarly, η_{inj} = carrier-injection-efficiency (CIE) strongly depends on the type and design of p-MQB EBL as well as distribution/modulation of Al-composition for suitable design of ud-AlGaN FB for potential height optimization. Furthermore, η_{inj} strongly depends on highly activated Mg-doped polarized p-AlGaN HIL as well as p-AlGaN contact layer of the UVB LEDs [3-4, 24-25, 38-39] and polarizibilty in the ud-AlGaN HIL too [42]. Similarly, the η_{lee} = light-extraction-efficiency (LEE), also strongly depends on the quality of highly transparent p-AlGaN HIL as well as p-AlGaN contact layer [24-35]. Furthermore, highly reflective p-electrode (mirror like), lenses structure, photonic crystal (PhC) either in p-AlGaN HIL or in p-GaN contact are also important for the enhancement of η_{lee}.[40-41]. The light extraction also depends on the special design, shapes and sizes of nano-structures in the sapphire or in the AlN template for the purpose of both total-TDDs reduction and for better light scattering in the UVB LEDs [3-4,7-9, 24-25, 40-41]. In order to enhance the η_{int} in UVB MQWs, first we need to know the level of total-TDDs in the n-AlGaN EIL underneath the MQWs. In the next subsection 3.1, we will focus on the crystallinity of UVB LEDs.

3.1 Crystallinity investigation, Al-alloy composition, and relaxation of n-AlGaN EIL of (300-310nm)-Band UVB LEDs

In this section, first the results of n-AlGaN BLs including n-AlGaN EIL relaxation, composition and crystal quality are deeply discussed. The large lattice-mismatch (LM) of 14% between C-Sapphire substrate and AlN template as well as the LM of 2.8 % between AlN template and AlGaN, respectively, caused to the generation of high TDDs in both the n-AlGaN EIL as well as in MQWs too. Such high level of TDDs in the MQWs were deteriorated to the η_{int} in the active region [3,8]. Significant fluctuations in local composition might occur due to decomposition of the ternary compound. This phenomenon is important in InGaN exhibiting a large miscibility gap [43], which strongly hinders the deposition of InGaN epilayers and MQWs with "In" content above ~ 20%. Meanwhile, calculations show that the AlGaN system is completely miscible [44], and $Al_xGa_{1-x}N$ epilayers are grown with Al content from $x = 0$ to1. AlGaN phase separation in the AlGaN materials were reported by Cremades et al. [45] for the first time. On the other hand, Marques et al. omitted to the indication of a miscibility gap in the AlGaN alloys, due to the smaller LM between AlN and GaN [46]. Even, the question about the issue of compositional phase separation in the AlGaN alloys due to the internal strain is still there and nevertheless, we have to rely on the concept of kinetic separation in the AlGaN materials. As the phase separation in the AlGaN were reported by Cremades et al. [45], and

1
2
3
4
5
6
7
8
9
10
11
12
13
14
15
16
17
18
19
20
21
22
23
24
25
26
27
28
29
30
31
32
33
34
35
36
37
38
39
40
41
42
43
44
45
46
47
48
49
50
51
52
53
54
55
56
57
58
59
60

however, the Marques et al. [46] negated to his claim (Cremades et al.) indirectly. Therefore, the possibility that the phase separation may not be neglected is still an ongoing debate among III-V researchers. In the DUV and UVB emitters, where the EL peak broadening or double peak emission from the MQWs may be speculated due to a localized energy states, which is attributed to kinetic separation in AlGaN crystal [26, 43, 46-48]. This is exceedingly difficult to precisely observe such crystal irregularities in the MQWs structure of AlGaN UVB LEDs, by using transmission-electron-microscopy (TEM) or three-dimensional atom probe [24]. The strain-relaxation condition in the n-AlGaN EIL may leads not only to the generation of extended defects and crystal irregularities in the MQWs, but it can excite to 3D growth mode in the AlGaN materials [26, 47-48].

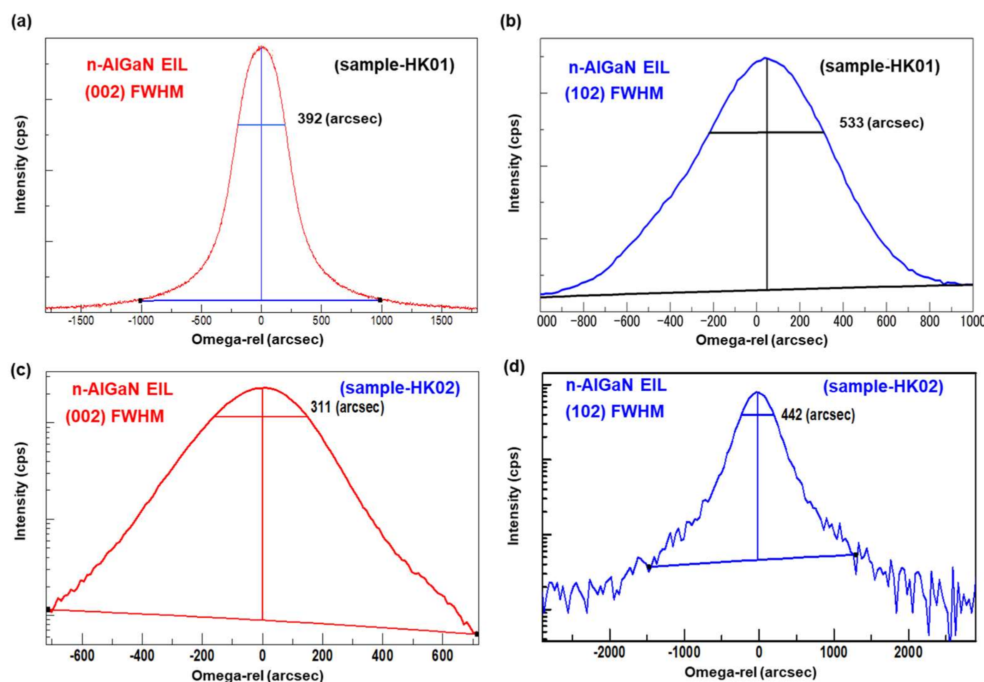

Fig. 2. The XRD-Rocking curves (XRCs) of the n-AlGaN EIL, where the FWHM values of (a) (0002) plane, and (b) (10-12) plane of sample-HK01 underneath the MQWs are given. The XRCs of the n-AlGaN EIL, where the FWHM values of (c) (0002) plane, and (d) (10-12) plane of sample-HK02 based on sample-A in Ref [4] underneath the MQWs are given. Figures: (c) and (d) reproduced from [4]. © 2019 Wiley-VCH Verlag GmbH & Co. KGaA.

To make a long story short, we have several choices of crystal growth strategies (routes), to suppress all possible types of TDDs, 3D growth modes, localized energy state or kinetically separated part in the n-AlGaN EIL grown on AlN template. Among such routes, either to grow crystal of AlGaN-based supper-lattices (SLs) structure as a buffer layer on AlN or to implement a crystal growth technique for the growth of thicker and highly relaxed stacking layers of n-AlGaN BLs including highly relaxed n-AlGaN EIL (without using SLs). More realistic could be high strain in the grown crystals, which give rise not only to the generation of high level of TDDs, however gives rise to a 3D growth modus and then a Ga-enrichment at the “macro-steps” [26, 47-49]. Previously, we successfully overcame the double peak EL emission from UVA and UVB-MQWs after reduction of total-TDDs either by using SLs based n-AlGaN BLs or either using Ga-rich and stacking of thick n-AlGaN BLs underneath the MQWs [26, 49]. Which give us the indirect evidence of 3D mode suppression or localized energy states inside the MQWs of UVA and UVB emitters. In order to get NB-UVB EL

1
2
3
4
5
6
7
8
9
10
11
12
13
14
15
16
17
18
19
20
21
22
23
24
25
26
27
28
29
30
31
32
33
34
35
36
37
38
39
40
41
42
43
44
45
46
47
48
49
50
51
52
53
54
55
56
57
58
59
60

emission for the medical applications, we need to overcome the aforementioned issues in the AlGaN crystal growth of MQWs.

In this paper, engineering of low total-TDDs and suppression of the 3D growth modus or kinetic separation in the n-AlGaN EIL underneath the MQWs of UVB LEDs for both 310nm emission and 300nm emission are investigated. The total-TDDs in the n-AlGaN EIL underneath the MQWs is particularly important for the enhancement of η_{int} as well as EL emission peak narrowing. Prior to the growth of (300 - 310nm)-band UVB LED devices, n-AlGaN EIL with low total-TDDs underneath the MQWs are quite critical for realizing high η_{int}, as demanded by Eq. (3). For 310nm-band UVB LED, a 200nm-thick and 50%-relaxed n-AlGaN EIL grown on the over layer of 3.4μm-thick n-AlGaN BLs in sample-HK01, where the FWHM of XRCs along (0002) and (10-12) planes respectively were controlled to approximately 392 arcsec and 533 arcsec (total-TDDs approximately ~7-8×10^8 cm^{-2}), shown in Figs. 2(a)-(b). Similarly, for 294nm-band UVB LED, a 200nm-thick and 32%-relaxed n-AlGaN EIL grown on the over layer of stacks of 1.7μm-thick n-AlGaN BLs sample-HK02 (similar to the sample-A in Ref [4]), where the FWHM of XRCs along (0002) and (10-12) planes respectively were reduced to approximately 311 arcsec and 442 arcsec (total-TDDs approximately ~6-7×10^8 cm^{-2}), shown in Figs. 2(c)-(d).

Furthermore, the crystalline quality of n-AlGaN BL and n-AlGaN EIL including the MQWs and p-MQB EBL of 310nm-band UVB LED were also investigated by using HR-TEM. In order to see all types of total-TDDs in n-AlGaN EIL of sample-HK01 (similar to sample-A in Ref [25]), the electron incidence direction was set to <10-10> zone axis for the images in Figs. 3(a)-(c). Figs. 3(a)-(b) and Fig. 3(c) include both g = [0002] (screw type) and g = [10-20] (edge and mixed type) vector information respectively for the estimation of total-TDDs. The evaluated TDDs types and values at Point-A of the sample-HK01 in the n-AlGaN EIL have been estimated. The edge-, screw-, and mixed-type TDDs, respectively, were confirmed to be 4.5×10^8, 5.5×10^7, and 4.7×10^7 cm^{-2} (estimated total-TDDs approximately ~ 7 ×10^8 cm^{-2}) in the n-AlGaN EIL structure underneath the MQWs. However, some unknown TDDs were also identified during the TEM measurement, which is marked in the white circle and shown in the inset of Fig. 3(a). Therefore, we underestimated the total-TDDs to be approximately ~ 7 ×10^8 cm^{-2} in the n-AlGaN EIL. This estimated total-TDDs are in close agreement with the XRCs data of sample-HK01 and such reductions of the total-TDDs might be caused by slightly relaxed n-AlGaN BL (relaxation ratio ~ 42%) as well as partially relaxed n-AlGaN EIL (relaxation ratio ~ 50%), shown in Fig. 4(a). The result of n-AlGaN EIL with low total-TDDs ~ 7×10^8 cm^{-2} of sample-HK01 are promising for improving the η_{ext} of (294-310nm)-band UVB LED and UVB LD devices [50]. There is strong relationship between the level of total-TDDs and the η_{int} [38-39].

The magnified RSM image of sample-HK01 has been shown in Fig. 4(a). The RSM indicates that the relaxation ratio approximately ~ 42% in the first n-type $Al_{0.55}Ga_{0.45}N$ BL and approximately ~ 50% in the final n-type $Al_{0.44}Ga_{0.56}N$ EIL, respectively, with respect to fully relaxed AlN substrate were successfully controlled, as shown in Fig. 4(a). Such relaxation of 50% in the EIL strongly influence the relaxation condition as well as piezoelectric field in the MQWs. Similarly, the magnified RMS image of sample-HK02 is shown in Fig. 4(b), where the first n-type $Al_{0.60}Ga_{0.40}N$ BL and second n-type $Al_{0.48}Ga_{0.52}N$ EIL of UVB LED, respectively are in a relaxed state with relaxation ratio of approximately ~ 20% and 32% with respect to fully relaxed AlN substrate. These reduced total-TDDs and relatively relaxed n-AlGaN EILs underneath the MQWs were aimed for the achievement of high η_{int} in the UVB LEDs.

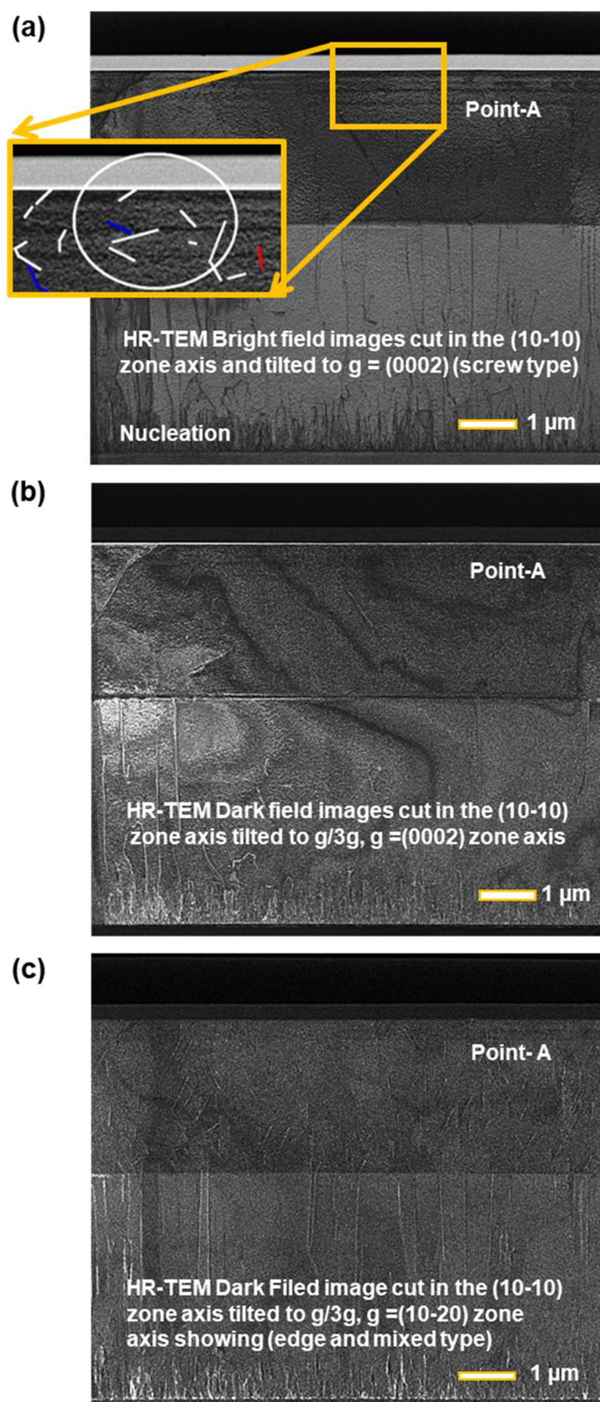

Fig. 3. (a) In order to see the screw type dislocations (some unknown TDDs inside the white circle has been shown in the inset), the cross-sectional HAADF-STEM images was cut in the (10−10) zone axis and tilted to g = (0002), and (b) cross-sectional TEM images cut in the (10−10) zone axis and tilted to the g/3g, *g* = (0002) zone axis. And, (c) similarly, to see the edge and mixed type dislocations at Point-A of sample-HK01, cross-sectional TEM images was cut in the (10−10) zone axis and tilted to the g/3g, g = (10−20) zone axis.

1
2
3
4
5
6
7
8
9
10
11
12
13
14
15
16
17
18
19
20
21
22
23
24
25
26
27
28
29
30
31
32
33
34
35
36
37
38
39
40
41
42
43
44
45
46
47
48
49
50
51
52
53
54
55
56
57
58
59
60

We also investigated the influence of thickness of n-AlGaN BL (T_{BL}) on the relaxation of n-AlGaN EIL underneath the MQWs for design of UVB emitters in sample-HK01, as shown in Fig. 4(c). The relaxation ratio in the n-AlGaN EIL underneath the MQWs increases with increase in thickness of buffer layer (T_{BL}), shown in Fig. 4(c). Such relaxation is critical for suppression of extended defects as well as non-uniformity in the Al-alloy distribution in the active region (MQWs) for the desired target of NB-UVB emission wavelength [26, 49]. Theoretically speaking one can see that there is a simple evaluation method to investigate the electric field dependence in a MQWs on the strain-relaxation condition [8, 52-53]. As we know that the total polarization field of an AlGaN layer can be expressed as given in the following Eq. (4) as:

$$P = P_{pz} + P_{sp} = \left(e_{31} - \frac{c_{13}}{c_{33}} e_{33}\right)\left(\frac{a_s}{a_e} - 1\right) + P_{sp}, \qquad (4)$$

where P_{sp} and P_{pz} are the spontaneous and piezoelectric polarization. Similarly, a_e : in-plane lattice constant of the unstrained epilayer, and a_s : in-plane lattice constant of a virtual substrate. The e_{31} and e_{33} are the piezoelectric constants, and c_{13} and c_{33} are the elastic coefficients in the AlGaN materials. As we know that the strain relaxation is proportional to a_s, and therefore the dependence of the polarization field on relaxation can be evaluated by taking the derivative of the total polarization with respect to a_s, as given in the following Eq (5) as:

$$\frac{dP}{da_s} = 2\left(e_{31} - \frac{c_{13}}{c_{33}} e_{33}\right)\left(\frac{1}{a_e}\right). \qquad (5)$$

By plugging the data of structural information in Eq. (5), the dependence of electric field on the relaxation (dP/da_s) was evaluated as a function of Al-composition and it turns out to be always negative. It was found that, the electric field was enhanced with the relaxation condition in an MQW (fully strained GaN/AlN are exempted), which reduce the overlap integral of electron and hole wave function in the MQWs. It can be speculated that the highly relaxed n-AlGaN EIL up to 80-90% might be useful for the UVA emitters [49], and partially relaxed n-AlGaN EIL up to 50% might be useful for the UVB emitters (this work). As a proof of concept, using 84% relaxed n-AlGaN EIL underneath the UVA-MQWs, we successfully achieve a η_{int} of 53% for UVA emitters [49]. In more simple word, we need different relaxation condition in the n-AlGaN EIL underneath the UVA, UVB and UVC-MQWs for different peak position of wavelength emission from UVA, UVB, and UVC emitters.

Also, for high η_{int} in the UVB LEDs, atomically flat and uniform interfaces between the QWB and QW are strongly desired. The 310nm-band UVB LED structure (sample-HK01) were investigated by using HR-STEM, as shown in Figs. 5(a)-(b). AlGaN-based layer by layer structure and different region of the UVB LED (n-AlGaN EIL/MQWs/ud-AlGaN FB, and p-side of the device including p-MQB EBL/p-AlGaN HIL) were clearly identified in the ABF-STEM image, as shown in Fig. 5(a). Furthermore, as shown in the HAADF image of Fig. 5(a), where noticeably clear, uniform and atomically smooth interfaces between the AlGaN-QWBs and AlGaN-QWs of MQWs were confirmed. Also, at the atomic resolution level layer by layer structure of III-V crystal were confirmed, as shown in Fig. 5(b), and ultimately [0001]-oriented G-face wurtzite crystal toward the p-AlGaN side was controlled. Due to the suppression of total-TDDs in AlN as well as in the underlying n-AlGaN EIL of MQWs, a very sharp and smooth interfaces between the QW and QWB in the UVB-MQWs were realized, as shown in Fig. 5(a) and 5(b). In the next subsection 3.2, the device performances of the 310nm and 294nm UVB LED devices are evaluated.

1
2
3
4
5
6
7
8
9
10
11
12
13
14
15
16
17
18
19
20
21
22
23
24
25
26
27
28
29
30
31
32
33
34
35
36
37
38
39
40
41
42
43
44
45
46
47
48
49
50
51
52
53
54
55
56
57
58
59
60

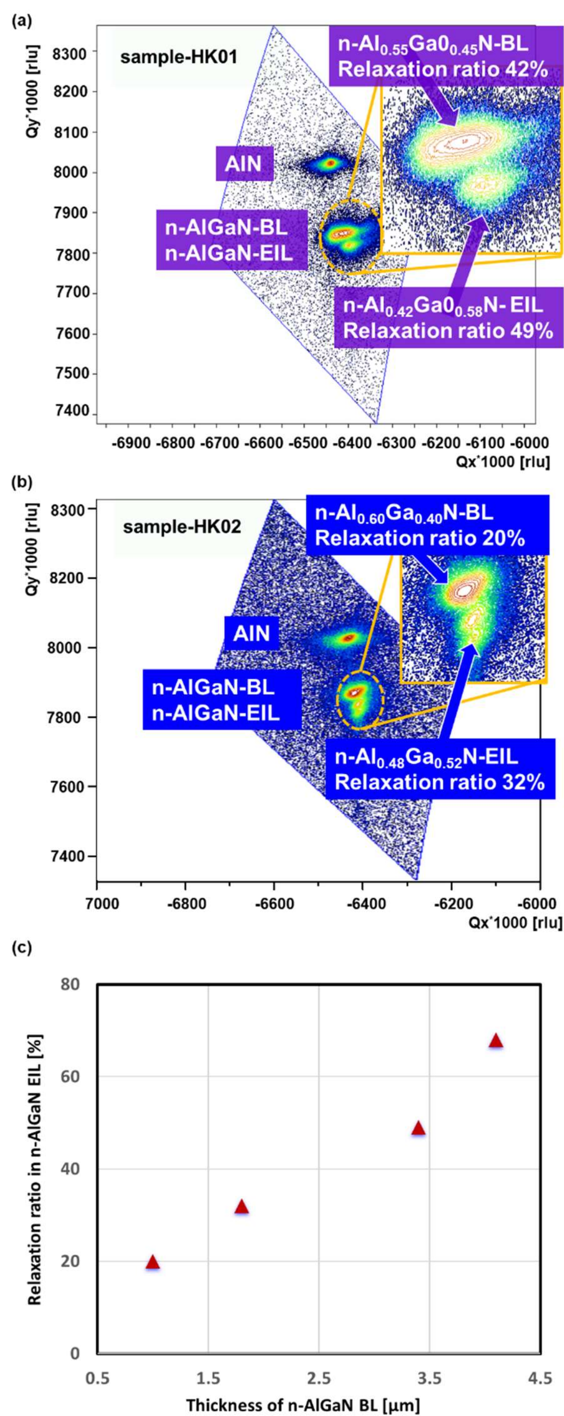

Fig. 4. (a) Reciprocal space mapping (RSM) along (105) reflections of the n-AlGaN EIL and n-AlGaN BL grown on an AlN template overlayer of (a) sample-HK01, (b) sample-HK02, and (c). The relationship between n-AlGaN BL thickness and relaxation condition in the n-AlGaN EIL.

1
2
3
4
5
6
7
8
9
10
11
12
13
14
15
16
17
18
19
20
21
22
23
24
25
26
27
28
29
30
31
32
33
34
35
36
37
38
39
40
41
42
43
44
45
46
47
48
49
50
51
52
53
54
55
56
57
58
59
60

3.2 Performance evaluation of 310nm-Band UVB LEDs

The electrical characterization results of the 310nm-UVB LED (sample-HK01) devices, as shown in Fig. 1(a) were discussed and compared with our previous results of 310nm-band UVB LED [3], shown in Figs. 5(c). Highly conductive n-AlGaN EIL underneath UVB-MQWs is essential for the smooth current injection into the active region (MQWs) of UVB emitters. Highly conductive n-AlGaN EIL underneath the UVB-MQWs (sample-HK01), where the electron concentration up to 4×10^{18} cm^{-3} and electron mobility up to 90 cm^2/V.s were controlled at RT. The resistivity around 2.06×10^{-2} Ω.cm in the n-AlGaN EIL at RT was also measured.

Previously, we observed some nonlinear behavior in the emitted L at 310 nm emission in UVB LEDs [3, 25], as well as at 326nm emission in UVA LED devices too in Ref [49] and it was determined that these nonlinearity in the $I–L$ and I-η_{ext} characteristics were not influenced either by varying number of stacking layers in AlGaN BLs or by using different materials (Ni/Au, Ni/Mg and Ni/Al) for p-electrodes [3, 49]. However, the reason of such nonlinear behavior in the $I–L$ and I-η_{ext} characteristics were attributed to the 25nm-thicker QWBs in the MQWs. Such thicker QWBs are preventing to the uniform distribution of e-h pairs in the MQWs region, which ultimately causes to inefficient radiative recombination in the active region of UVB LEDs [51]. Therefore, we suspected that the nonlinearity in the I-L and I-η_{ext} of the 310nm-band UVB LED might be linked to un-optimized thickness of QWB (T_{QWB} ~ 25 nm), which might be the root cause of poor hole transport as well non-uniform distribution of e-h pairs inside the MQWs at low current injection [3-4, 51]. When, the structure thickness of QWB (T_{QWB} ~ 25 nm) in sample-A [25], was reduced to approximately 8-10nm in the revised 310nm-band UVB LED (sample-N) [3], the issue of nonlinearity in the I-L and I-η_{ext} were overcome. The sample-N with a conventional Ni/Au p-electrode was demonstrated, where single peak EL spectral emission at 310nm was confirmed. The maximum L was increased from 7.1mW [25] to 13 mW [3], and similarly the maximum η_{ext} was greatly improved from 0.5% [25] to 2.3% on bare-wafer condition under the CW-operation at RT in sample-N, shown in Fig. 5(c). Previously, in all samples of 310nm-band UVB LEDs including the best sample-N, where 32% relaxed n-AlGaN EIL underneath the MQWs were used [3, 25]. However, in this work it was found that the 3.4 µm-thick n-AlGaN BL and 50% relaxed n-AlGaN EIL grown on AlN template (sample-HK01) serves as a pseudo-substrate, and it might release the strain to QWBs of the MQWs. Furthermore, by this way of releasing the strain to the MQWs, one can suppress the extended defects or any Al-alloy fluctuation in the active region of UVB LEDs [49]. The first QWB between n-AlGaN EIL and MQWs is particularly important for stress reliving support and also to suppress the piezoelectric field in the MQWs [8,34,49]. The underlying 50%-relaxed n-AlGaN EIL is key to further suppress the total-TTDs and piezoelectricity in UVB-MQWs [49]. The same influence of relaxation in the n-AlGaN EIL on the piezoelectricity in the MQWs was confirmed by simple evaluation model, as given in Eq. (4) and (5).

In the revised sample-HK01, the thickness of all QWBs were reduced from 25nm to 10nm and highly reflective mirror like 1nm-thick Ni / 200nm-thick Al (having reflectance ~ 84%) p-electrodes were deposited on p-AlGaN contact layer for the enhancement of η_{lee}, as shown in the inset of Fig. 6(c) and 6(d). The chip sizes of the Ni/Al p-electrodes were chosen to be 200×200, 300×300, 350×350, and 400×400 μm^2, respectively, as shown in the inset of Fig. 6(c) and 6(d). The performances of 310nm-band UVB LEDs was evaluated at RT under both CW- and pulse-operation using chip size area of 300×300 μm^2 and 200×200 μm^2 on bare-wafer condition, respectively, shown in Figs. 6(a)-(d). The inset of Fig. 6(b) shows the EL spectra of sample–HK01 at RT, where single peak emissions at 310nm were confirmed with the FWHM of the emitted UVB-Light about 12 nm. This UVB light emission with FWHM around 12 nm is quite near to the desired target value of NB emission of 4-5nm for medical applications, however some more improvement in the band-narrowing of UVB light is needed.

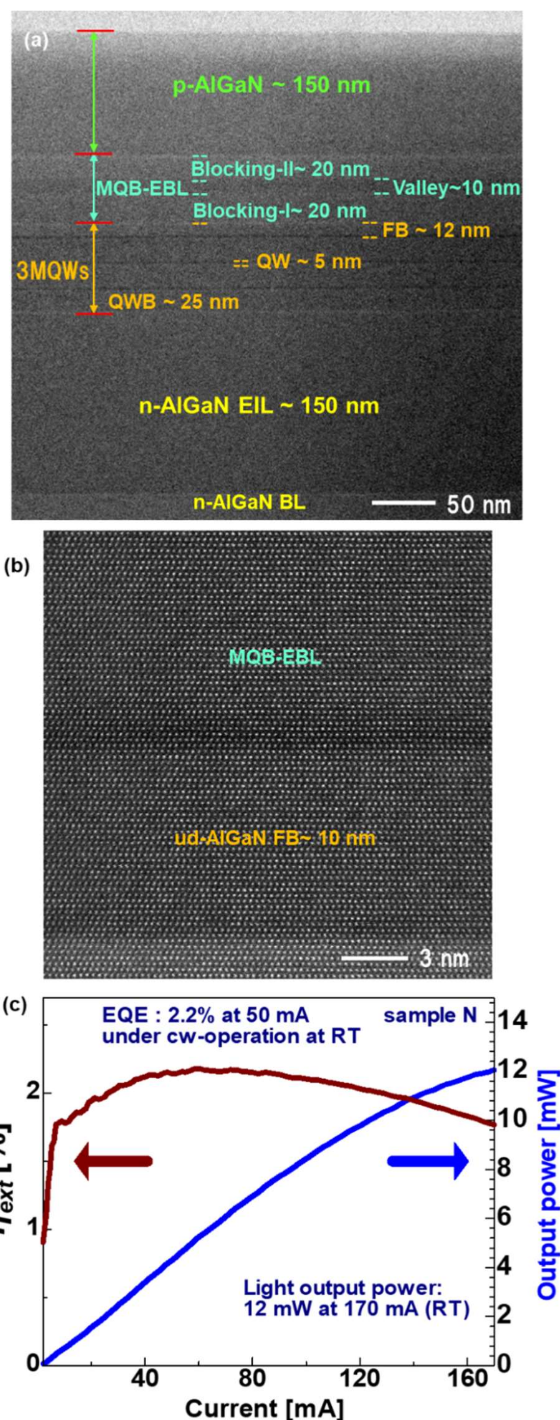

Fig. 5. (a) Magnified ABF-STEM images of sample-A LED structure, (b) magnified HAADF-STEM images of sample-A Ref [3], and performance evaluation of the 310nm-band UVB LED (sample-A): (c) current vs output power (*I–L*), current vs η_{ext} (*I*-η_{ext}) characteristics at RT [3]. Figures: (a), (b) and (d) reproduced from [3]. © 2020 The Japan Society of Applied Physics.

1
2
3
4
5
6
7
8
9
10
11
12
13
14
15
16
17
18
19
20
21
22
23
24
25
26
27
28
29
30
31
32
33
34
35
36
37
38
39
40
41
42
43
44
45
46
47
48
49
50
51
52
53
54
55
56
57
58
59
60

The possibility in the broadening of EL might be attributed to several potential reasons. On one hand by increasing the Al-allow difference between QW and QWB improves the carrier confinement but on the other it could potentially increase the emission peak broadening due to the increase of the piezoelectric polarization. Also such EL peak broadening is due to the non-uniform thickness of the QW at nanometer scale in threefold MQWs structure, which means that the slight shift in the band gap of first QW from the second QW can ultimately give rise to the broadening in the EL emission peak. Most importantly, the carrier localization phenomenon can substantially affect the carrier dynamics in AlGaN epitaxial layers and quantum well structures too. The origins of the carrier localization in AlGaN were discussed more broadly by Tamulaitis et al. [52], who found that the carrier localization can severely influence the efficiency of the radiative and non-radiative recombination of non-equilibrium carriers [52]. It is generally accepted that the lattice constants of $Al_xGa_{1-x}N$, as well as of many other semiconductor compounds, follow the Vegards law and linearly increase from their values in GaN down to those in AlN as x in $Al_xGa_{1-x}N$ increases from 0 to 1. The alloy in AlGaN has intrinsic composition fluctuations due to random spatial distribution of Ga and Al cations in AlGaN lattice crystal.

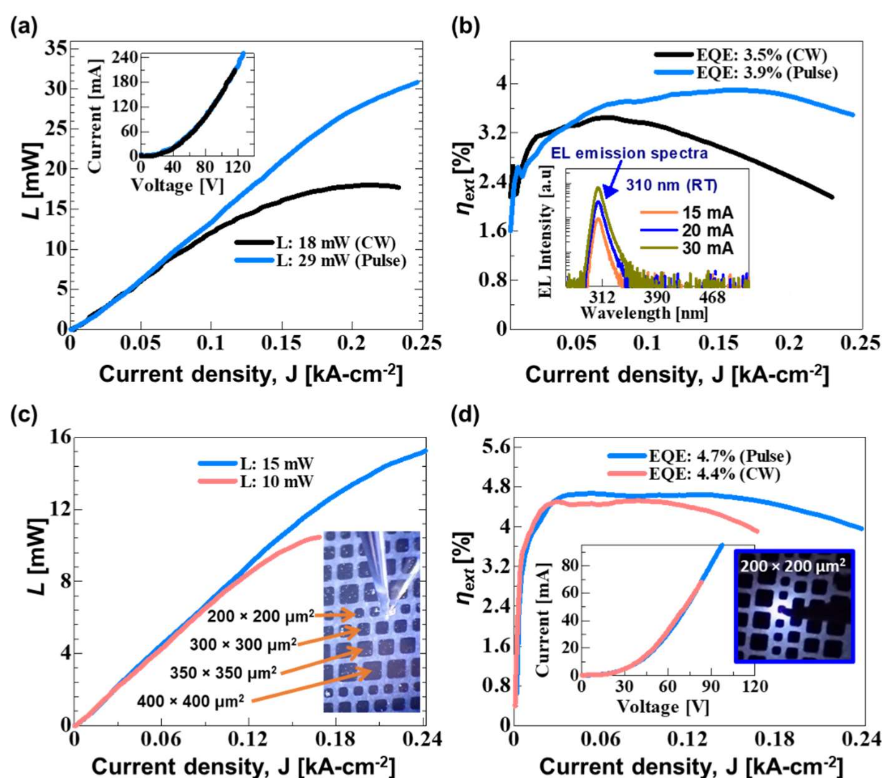

Fig. 6 Performance evaluation of the 310nm-band UVB LED (sample-HK01): (a) current vs output power (I–L) characteristics of UVB LED with big chip (*I-V* characteristics are shown in the inset), (b) current vs η_{ext} (I-η_{ext}) characteristics (An image of real UVB LED with 300×300 μm² size chips is shown in the inset of Fig. 6(c)) and single peak EL emission spectra are also shown in the inset, (c) current vs output power (*I–L*) characteristics (an image of real UVB LED with small chip 200×200 μm² size is shown in the inset), and (d) current vs η_{ext} (I-η_{ext}) characteristics on bare-wafer level measurement (*I-V* characteristics and real small device during operation are shown in the inset).

1
2
3
4
5
6
7
8
9
10
11
12
13
14
15
16
17
18
19
20
21
22
23
24
25
26
27
28
29
30
31
32
33
34
35
36
37
38
39
40
41
42
43
44
45
46
47
48
49
50
51
52
53
54
55
56
57
58
59
60

Broadening of the PL band at low temperatures is the most straightforward signature of the alloy fluctuations in the MQWs too. Tamulaitis et al. found that the increase in FWHM of the PL band is proportional to the standard deviation of the bandgap [52]. Broadening of the EL spectra, which is accompanied by a redshift can be attributed to the overlapping of spectral structures in the MQWs. Similarly, carrier localization in both the 295nm and 310nn-band UVB MQWs of UVB LEDs may give rise to the peak broadening of EL spectral emission [26]. More rationally the highly strained crystals can give rise to 3D growth modus and subsequently to Ga-enrichment region could occur at the "macro-steps" [26, 47-48]. Therefore, for the narrowing of EL spectrum from FWHM of 12nm to 4nm, we need to overcome the issues of alloy fluctuation, generation of 3D mode as well as any localized energy state in the MQWs. Also, strictly control of the QW's thickness as well as Al-contents in all threefold MQWs will be essential too [53].

Furthermore, after using an 50% relaxed n-AlGaN EIL underlying the MQWs and assisted by reduction of the T_{QWB} in the MQWs of UVB LED from 25nm to 10 nm (sample-HK01), then the maximum L was greatly improved from 13 mW [3] to a record value of 18 mW (this work) under CW-operation at RT, using chip size of 300×300 μm^2, shown in Fig. 6(a). Similarly, a remarkable improvement in the L up to 29 mW (this work) under pulse-operation (with low heating of the device) was achieved, shown in Fig. 6(a). Subsequently, the maximum η_{ext} was drastically improved from 2.3% (sample-N) in Ref [3] to 3.5% (sample-HK01) under CW-operation at RT using chip size of 300×300 μm^2, shown in Fig. 6(b). Furthermore, the maximum η_{ext} were greatly enhanced up to 3.9% (sample-HK01) under pulse-operation at RT, chip size: 300×300 μm^2, shown in Fig. 6(b). When we used a small chip (200×200 μm^2) of Ni/Al p-electrode (shown in the inset of Fig. 6(c)), the maximum value of L about 16 mW under pulse-operation was demonstrated. Subsequently, the maximum η_{ext} was remarkably enhanced to a record value of 4.7% at 310nm emission (sample-HK01) under pulse-operation, shown in Fig. 6(d). However, high operating voltages (20-30V) under 20 mA were observed in the sample-HK01 due to the Ni/Al p-electrodes and In-dot n-electrode (bare-wafer condition), as shown by the *I-V* characteristics given in the inset of Fig. 6(a) and Fig. 6(d). On one side the Ni/Al gives high operating voltages but on the other side it gives quite high reflectivity for UVB light from the mirror like Ni/Al p-electrodes. The low activated Mg-atoms in the p-AlGaN HIL including p-AlGaN contact layer is also one of the reasons of high operating voltages in these devices.

We also compared the relative transmittances of the emitted UVB lights via p-AlGaN HIL including p-AlGaN contact layer and reflectance from different types of p-electrodes, which were used in the previous UVB LED devices [3-4, 24-25]. Previously, for relative comparison of the reflectance, different p-type of electrodes, where Ni(1nm)/Mg(200nm), Mg(200nm), Ni(1nm)/Al(200nm), and Ni(30nm)/Au(150nm) stacking layers, respectively, were grown directly on the C-Sapphire substrates and then it was calibrated by the reflectance of an AlN/sapphire reference sample. The measured values of the relative reflectivity were found approximately to be 100% (Mg), 88% (Ni/Mg), 84% (Ni/Al), and 34% (Ni/Au) for UVB LEDs applications and the detail about such investigation is given in the supplementary information of Ref [25]. Ultimately, we found that the new structure of 1nm-thick Ni layer flowed by 200nm-thick Al layer as a highly reflective and such oxide free p-electrode (this work) is quite promising for mirror like reflection of UVB light, shown in the inset of Fig. 6(c) and Fig. 6(d). In this comparative study of reflectivity and operating voltages, it was found that we need some tradeoff between high reflectivity as well as low operating voltages. However, the issue of high operating voltages and non-ohmic contact in the UVB LEDs are still remaining. One most suitable solution is to opt for the flip-chip (FC) technology to fabricate low resistive *p (n)*-electrodes in the UVB LED devices. The FC technique, which is based on Ti/Al/Ti/Au (n-electrode) and Ni/Au (p-electrode) has already been realized in our lab for UVC LED at 270 nm emission [40-41,54]. The same technique of FC-based n-electrode could

1
2
3
4
5
6
7
8
9
10
11
12
13
14
15
16
17
18
19
20
21
22
23
24
25
26
27
28
29
30
31
32
33
34
35
36
37
38
39
40
41
42
43
44
45
46
47
48
49
50
51
52
53
54
55
56
57
58
59
60

possibly enhance the performances of the existing 310nm-band UVB LED devices by several fold with reduced operating voltages. Such issues of the UVB LED devices including FC will be discussed in the section-(4) of this paper. In the next subsection 3.3, performance evaluation of 294nm-band UVB LED devices are discussed.

3.3 Performance evaluation of 294nm-Band UVB LEDs

First the optical characterization and then device characterization of 294nm-band UVB LEDs (sample-HK02) for certain medical and agriculture application in mind are discussed. We will briefly discuss about the current status and progress of 294nm-band UVB LEDs at Riken [3-4, 24-25]. The IQE (η_{int}) of 294nm-band UVB LED devices were evaluated and then compared to our previous results [3-4, 24-25], as shown in Fig. 7(a)-(b) and Fig. 8(a). Previously, the η_{int} of the AlGaN UVB LED (sample-B) at emission wavelength of 294nm [25] was measured by standard measurement method given in Ref [35], and the results are shown in Fig. 7(a)-(b). The η_{int} curves of UVB LED (sample-B) at 10 K (dark circles) and at RT (blue circles), as a function of excitation-power-density under the excitation wavelength of 240 nm were measured, as shown in Fig. 7(a). The estimated η_{int} curves of 47% was achieved at RT, after normalizing by the maximum η_{int} at 10 K and the maximum η_{int} at RT. The integrated PL intensity of UVB LED (sample-B) was also measured

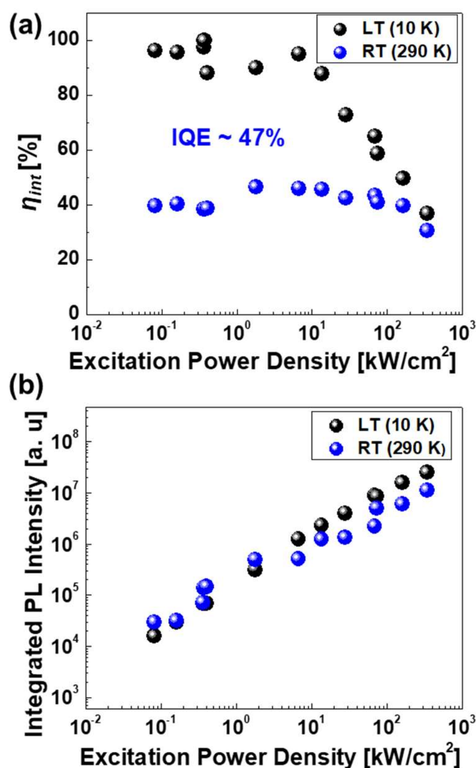

Fig. 7. (a) η_{int} vs excitation power density measured for sample-B [25], and (b) temperature-dependent of PL vs excitation power density measured for sample-B [25]. Figures: (a) and (b) reproduced from [25]. © 2019 The Royal Society of Chemistry (RSC).

and the PL intensity curves at 10 K (dark circles) and RT (blue) as a function of excitation-power-density has been shown in Fig. 7(b). We also observed that the η_{int} at a lower excitation-power-density remains constant, which indicates that non-radiative recombination centers freeze out at LT (10 K). Subsequently, the η_{int} were enhanced from our previous value of 40% [24] to 47% [25] in the UVB LED (sample-B) at emission wavelength of 295nm. Subsequently,

1
2
3
4
5
6
7
8
9
10
11
12
13
14
15
16
17
18
19
20
21
22
23
24
25
26
27
28
29
30
31
32
33
34
35
36
37
38
39
40
41
42
43
44
45
46
47
48
49
50
51
52
53
54
55
56
57
58
59
60

the maximum η_{ext} was also improved from 3.3% [24] to 4.4% [25]. Similarly, the maximum L was improved up to 13mW [25] after optimizing the thickness of the n-AlGaN EIL. But the maximum L of 13 mW was found to be still very low for the real-world applications to replace the toxic Mercury UVB-Lamp, therefore some more improvement in the performances (η_{ext}, η_{int}, η_{inj} and η_{lee}) of UVB light sources are greatly needed. In order to further improve the efficiency and light output power of UVB LEDs, then the MQWs as well as the energy band structure of the previous devices [24-25] as shown in Figs. 8(a)-(b), were re-investigated (this work), as shown in Fig. 1(c).

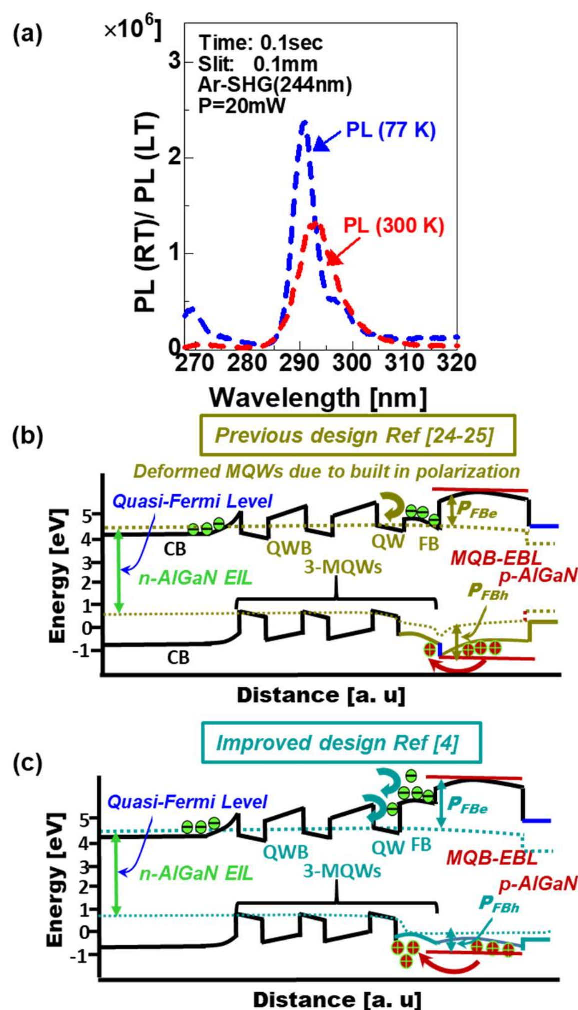

Fig. 8. (a) Integrated PL spectra of sample-A [4], measured using a 20mW Ar-SHG (244nm) laser as an excitation source both at RT (300K) and at low temperature (77K). (b) Schematic view of the energy band diagram of our previous 294nm-band UVB LED, where an un-optimized ud-AlGaN FB was used in Ref [24-25], and (c) Schematic view of the energy band diagram of our improved 294nm-band UVB LED, where optimized ud-AlGaN FB was used and the same optimized ud-AlGaN FB was used in sample-HK02. Figures: (b) and (c) reproduced from [4]. © 2019 Wiley-VCH Verlag GmbH & Co. KGaA.

It is well known that the η_{int} is strongly dependent on the point defects, undesired impurities (C, O, and H) as well as all type of TDDs in the AlGaN-based UVB MQWs [38-39]. It is also true, that the crystalline quality of MQWs is further dependent on the underlying

1 2 3 4 5 6 7 8 9 10 11 12 13 14 15 16 17 18 19 20 21 22 23 24 25 26 27 28 29 30 31 32 33 34 35 36 37 38 39 40 41 42 43 44 45 46 47 48 49 50 51 52 53 54 55 56 57 58 59 60

crystalline quality of n-AlGaN EIL [4, 25]. After suppressing the total-TDDs in n-AlGaN EIL of sample-A in Ref [4], as shown in Figs. 2(c)-(d), and then using the same n-AlGaN EIL in sample-HK02 (this work), then the photoluminescence's efficiency from the UVB-MQWs was greatly improved. Subsequently, the PL ratio at RT (PL_{RT}: 300K) and at low temperature (PL_{LT}: 77K) were estimated to be approximately ~ 54%, as shown in Fig. 8(a). It can reasonably be concluded that the decrease of the edge-type TDDs from 793 arcsec [24-25] to 442 arcsec (sample-A) [4], shown in Fig. 2(d), resulted in the increase of 7% of PL emission efficiency (PL_{RT}/PL_{LT}) from 47% [25] to 54% (sample-HK02). Previously, we used 48% Al-composition in the ud-AlGaN FB of sample-B [25], however in sample-A Ref [4], the Al-composition were also increased up to 55% in the ud-AlGaN FB, as shown in Figs. 8(a)-(c). However, one issue in the potential barrier height (P_{FBh}) of the ud-AlGaN FB and EBL-I (especially the potential barrier height for hole) of MQB EBL was found. The P_{FBh} of QWB in MQWs and ud-AlGaN FB of MQWs were found at the same level (Al-contents: 48%), and the same is indicated in Figs. 8(b) and 8(c), respectively, for sample-A in Ref [4] and sample-B in Refs [24-25]. Such situation at the interface of the p-MQB EBL and ud-AlGaN is not suitable for efficient hole injection toward the MQWs, as shown in Fig. 8(b). It is very important to mention here, that the newly designed UVB LED (sample-HK02), where the Al-composition approximately 55% in the ud-AlGaN FB was chosen, when compared to the Al-composition approximately 48% in the normal QWBs of the MQWs, for suppression of Mg-diffusion from p-MQB EBL toward the MQWs as well as for confining of low energy electron in to MQWs of UVB LED.

In this work, we introduce a moderately Mg-doped p-MQB EBL, as shown in Fig. 9(a) for better hole transport (to enhance the η_{inj}) from p-AlGaN HIL to MQWs via HIT and HTE in sample-HK02, and the schematic energy band diagram of the same has been shown in Fig. 1(c). The Mg-atomic depth profiles in the improved design of Mg-doped p-MQB EBL (sample-HK02), using SIMS measurement is shown Fig. 9(a). SIMS measurement shows that the newly designed ud-AlGaN FB between MQWs and p-MQB EBL successfully suppressed to the Mg-diffusion from MQWs, as shown in Fig. 9(a). Due to the low carrier confinement in the MQWs of sample-A, the η_{ext} of UVB LED was degraded [4], and therefore the UVB-MQWs was further optimized in the perspective of better carrier confinement. Especially, the Al-alloy difference between QWBs and QWs were increased from 15% (sample-A) [4] to 20% in newly grown MQWs of sample-HK02 for better carrier confinement as mentioned in the Ref [42] about the UVA-MQWs. Figure. 9(b) shows the real image of the UVB LED during the operation, where the In-dot n-electrode and Ni/Al p-electrode has been shown on bare-wafer condition. The estimated schematic energy band diagram including p-electrode contact of the UVB LED (sample-HK02) has been shown in Fig. 1(c).

Finally, the performances of sample-HK02 based UVB LEDs were evaluated at RT under both CW- and pulse-operation using highly reflective (86%) Ni/Al p-electrode, with chip size areas of 300×300 μm^2 and 200×200 μm^2 on bare-wafer condition, shown in Figs. 9(b)-(f). The inset of Fig. 9(d) shows the EL spectra of sample–HK02 with injection drive current range from 7 mA to 20 mA at RT. Single peak emissions at 295 nm were confirmed, where the FWHM of the emitted UVB-light was controlled around 10nm, and some improvement in the EL peak narrowing was observed, when compared to the EL emission peak at 310nm emission from sample-HK01. When the Al-contents were increased from approximately 15% (sample-A) of Ref [4] to approximately 20% (sample-HK02) as well as using p-MQB EBL, the maximum L was remarkably enhanced from 17 mW (sample-A) [4] to a record value of 32 mW on bare-wafer level measurement under pulse-operation at 295 nm emission (chip size: 300×300 μm^2), shown in Fig. 9(c). The inset of Fig. 9(c) and (e) gives the I-V characteristics of sample–HK02 at RT, which still shows high operating voltages. These high operating voltages are attributed to problematic p-AlGaN HIL and p-AlGaN contact layer, where Mg-atoms generates a very deep accepter energy level in the AlGaN crystal. Also, the measurement on bare-wafer condition give rise to high operating voltages too. Such issues of high operating

1
2
3
4
5
6
7
8
9
10
11
12
13
14
15
16
17
18
19
20
21
22
23
24
25
26
27
28
29
30
31
32
33
34
35
36
37
38
39
40
41
42
43
44
45
46
47
48
49
50
51
52
53
54
55
56
57
58
59
60

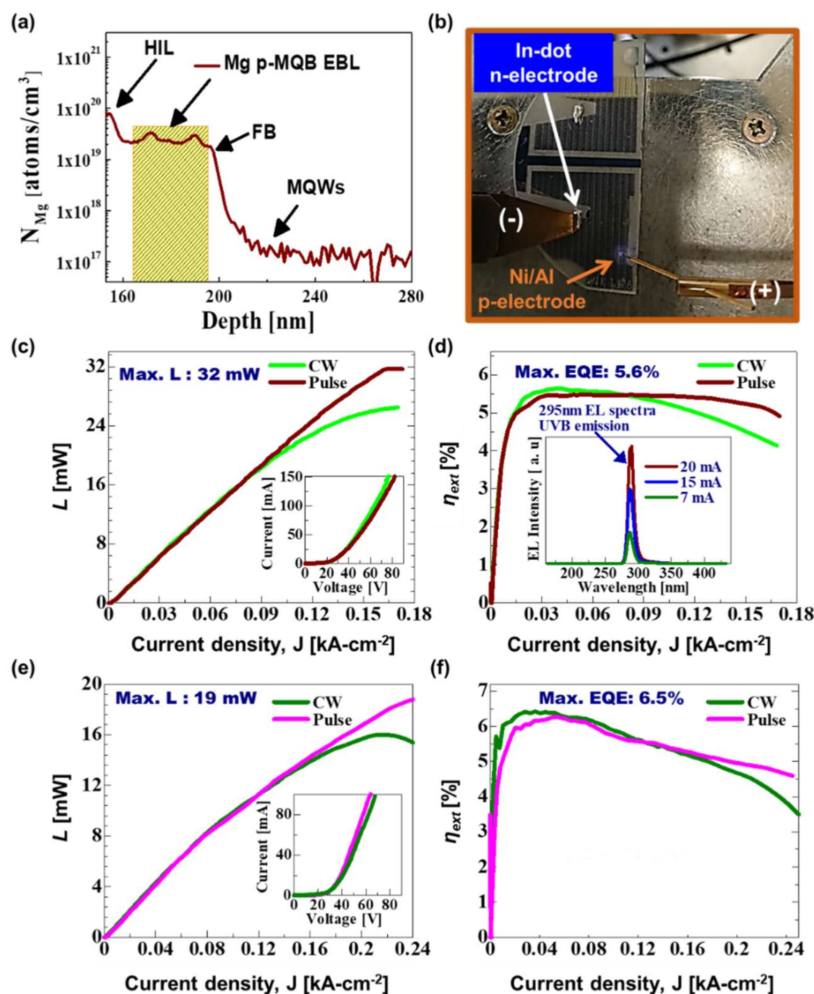

Fig. 9. (a) The SIMS depth profiles of Mg-atoms in the newly designed p-type MQB EBL (sample-HK02) at nanometer scale. Performance evaluation of the (294-300 nm)-band UVB LED (sample-HK02): (b) The real image of the UVB LED during the operation, where the In-dot n-electrode and Ni/Al p-electrode has been marked, (c) current vs output power (*I–L*) characteristics of 300×300 μm^2 size chip under both CW and pulse-operation on bare-wafer, (d) current vs η_{ext} (I-η_{ext}) characteristics of 300×300 μm^2 size chips (The single peak EL emission spectra are shown in the inset), (e) current vs output power (*I–L*) characteristics of 200×200 μm^2 size chip under both CW and pulse-operation on bare-wafer, and (f) current vs η_{ext} (I-η_{ext}) characteristics of 200×200 μm^2 size chips at RT.

voltages can be eased by using distributed Al-alloy for the polarizability in the p-AlGaN HIL [42] as well as fabricating of FC-electrodes on the devices [40-41]. The maximum η_{ext} were also improved up to 5.6% (sample-HK02: this work), using highly reflective Ni (1nm) /Al (200nm) p-electrode, on bare-wafer level measurement under CW-operation at 295 nm emission (chip size: 300×300 μm^2), shown in Fig. 9(d). Incredibly low droop in the η_{ext} were observed, as shown in the Fig. 9(d). This low droop is attributed to the improved hole transport due to hole by intraband tunneling (HIT) in p-MQB EBL as well as by using suitable size of p-electrode. The maximum L of 19 mW on bare-wafer level measurement under the pulse-operation at 295 nm emission (chip size: 200×200 μm^2) was obtained, shown in Fig. 9(e). Finally, the maximum η_{ext} were drastically improved from 5.6% (sample-A) [4] to a record value of 6.5% (sample-HK02: this work), using highly reflective Ni (1nm) /Al (200nm) p-

1
2
3
4
5
6
7
8
9
10
11
12
13
14
15
16
17
18
19
20
21
22
23
24
25
26
27
28
29
30
31
32
33
34
35
36
37
38
39
40
41
42
43
44
45
46
47
48
49
50
51
52
53
54
55
56
57
58
59
60

electrode assisted by new design of p-MQB-EBL under CW-operation at RT, shown in Fig. 9(e). If we compare the droop behavior in the η_{ext} of chip size: 200×200 μm^2 with that of chip size: 300×300 μm^2 using same sample under pulse-operation, it was found that smaller is the chip size area, larger is the droop in the η_{ext}, as shown in Fig. 9(d) and 9(f). For further improvement in both 310nm-band and 294nm-band UVB LEDs, to replace the toxic mercury UV-Lamp, few challenges are critically needed to be overcome, as demanded by Eq. (3). Especially, the issue of low hole injection efficiency toward the MQWs (η_{inj}) due to the low activation energy of Mg-atoms in both the p-AlGaN HIL and p-AlGaN contact layer of UVB LED, is inevitably needed to be resolved. The hole injection is the most challenging issue in the III-V materials-based UV emitters and such challenging issues including some other too will be discussed in the next section 4.

4. Challenges and Future Directions of AlGaN UVB emitters

Crystal growth and engineering of AlGaN-based UVB LEDs and LDs (with Al-composition around 35-45% in the AlGaN MQW) on AlN templates by using LP-MOVPE, are quite difficult due to the possibility of complex growth, i.e. 3D growth modus, localized energy states caused by kinetic separation and some crystal irregularities in AlGaN crystal [3-4, 7-9, 24-26, 47-48, 50]. Such crystal irregularities and complex growth in AlGaN, or extended defects in the MQWs as well as in the n-AlGaN EIL underneath the MQWs [26, 47-48] are quite problematic for all UV-emitters, including UVB LEDs and LDs. Recently, we successfully reduced to the total-TDDs to approximately ~ 6-7×10^8 cm^{-2} in the n-AlGaN EIL underneath the UVB-MQWs [4], using either partially relaxed or highly relaxed n-AlGaN BL and n-AlGaN EIL (relaxation ratio ~ 32-50%). Subsequently, a record η_{int} both in the AlGaN-based UVA- and UVB-MQWs, respectively, of 53-54% were achieved [4,49]. We need further improvement in the performances (η_{ext}, η_{int}, η_{inj} and η_{lee}) of AlGaN based UVB LEDs including LDs grown on AlN template with emitted light output power up to 400mW as well as with very low operating voltages of 4-6 V and high current density of 100 kA-cm^{-2}.

First, it is particularly important to realize a highly UV-transparent (high η_{lee}) p-AlGaN HIL and p-AlGaN cladding layer (CL) to replace highly opaque p-GaN layer for the UVB LED and LDs applications. Highly transparent p-AlGaN HIL and p-AlGaN contact layer are inevitable for the extraction of reflected UVB light from the mirror like p-electrodes (Ni/Mg or Ni/Al or Rh). In this work, the relative UV-light transmittance of more than 90% in the wavelength emission range from 290 nm to 320 nm through p-AlGaN UVB LEDs including sample-HK01 and sample-HK02 were confirmed [4,25], as shown in Fig. 10(a)-(b). Transmittance of more than 98% for an AlN/sapphire template with a sapphire substrate was first confirmed, as shown in Fig. 10(b). The relative transmittance gives the ratio between UV-light intensity transmitted through an UVB LED on an AlN/sapphire template and the UV-light intensity transmitted through the AlN/sapphire template only [35]. In order to replace the opaque p-GaN layers by transparent p-AlGaN layers for the enhancement of η_{lee} in the UVB LED and LD devices, then engineering of such highly transparent p-MQB EBL, p-AlGaN HIL/CL and p-AlGaN contact layer, respectively, are very essential.

In order to reduce the operating voltages as well as to enhance the hole injection in to the MQWs, we need to opt for both the FC technology [54] as well as highly conductive p-AlGaN contact layer including p-AlGaN HIL, using polarizability in the p-AlGaN layers [42]. As we know that the hole concentration "p" depends on the acceptor energy level in the exponential fashion as: $p \sim \exp\left(-\frac{E_A}{kT}\right)$, where k: Boltzmann constant, T: absolute temperature, and E_A: activation energy level (ranging in 400-500 meV) in the p-AlGaN HIL, as shown in Fig. 10(c). It can translate only one free hole for roughly every two billion (2 × 10^9) doped Mg-atoms in the p-AlGaN HIL at RT. In another words, it shows that the η_{ext} of UVB LEDs decreases exponentially with decreasing wavelength of the emitted UV light, as shown in Fig.

ACS Paragon Plus Environment

1
2
3
4
5
6
7
8
9
10
11
12
13
14
15
16
17
18
19
20
21
22
23
24
25
26
27
28
29
30
31
32
33
34
35
36
37
38
39
40
41
42
43
44
45
46
47
48
49
50
51
52
53
54
55
56
57
58
59
60

10(c). For UVB emitters, we need at least 2× 10^{16} cm^{-3} ”p” in the p-AlGaN HIL or p-AlGaN CL, as shown in Fig. 10(c).

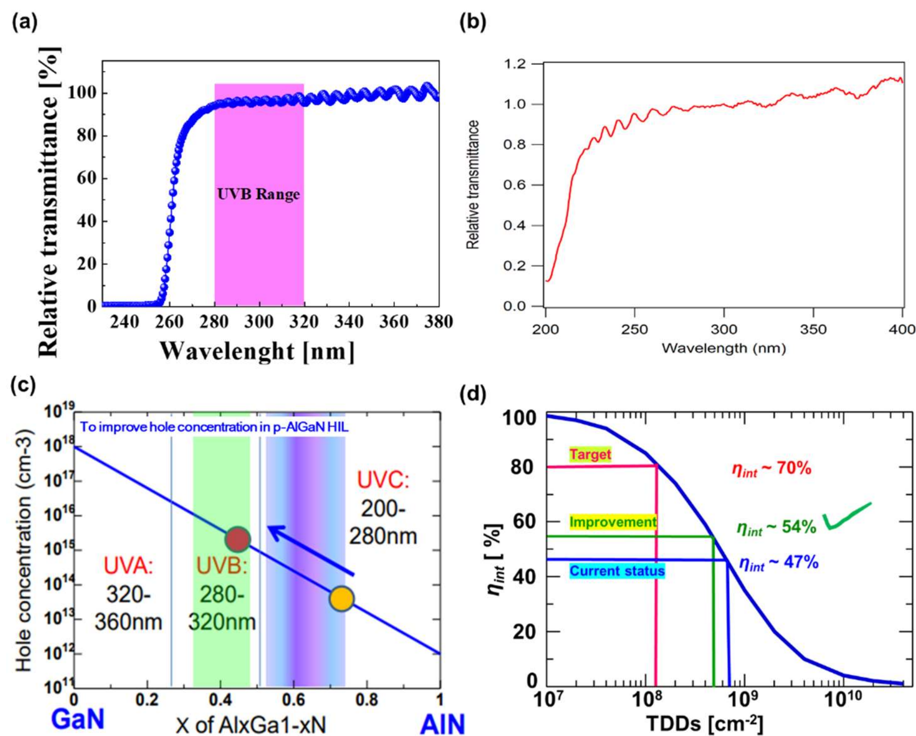

Fig. 10 (a) Relative transmittance [%] through p-AlGaN of UVB LED [25], (b) relative transmittance of an AlN/sapphire template with a sapphire substrate, (c) hole concentration Vs Al-composition in the p-AlGaN, and (d) Relationship between η_{inj} (IQE) and threading dislocation densities [39]. Figure: (a) reproduced from [25]. © 2019 The Royal Society of Chemistry (RSC). Figure: (d) reproduced from [39]. © 2010 The Japan Society of Applied Physics (APEX).

To activate the Mg-atoms in the p-AlGaN HIL or p-AlGaN CL we need some suitable annealing technique to replace the conventional rapid thermal annealing (RTA), without causing damage to the delicate MQWs structure of UVB LEDs. One new candidate could be excimer-laser-annealing (ELA), which is still under investigation for the activation of Mg-dopants in the p-AlGaN HIL including p-AlGaN contact layer under different environmental conditions i.e., in Ar, atmosphere, vacuum and N_2. ELA offers many advantages compared to the rapid thermal annealing (RTA) technique or high-temperature-annealing (HTA) technique, such as higher activation efficiency of dopants in the p-AlGaN and depth control over the junction depth [55-56]. ELA has one challenge of large area spot size of laser beam. In addition to the previous proposed solutions, some new heterostructure (HET) is also proposed for achieving high “p” in the p-side of UVB LED and LD devices. Such HET structure might be based on some new materials grown on p-AlGaN HIL in the UVB emitters. A novel HET structure of very thin p-type 2D material like hexagonal-Boron Nitride (p-hBN) assisted by Al-graded (polarized) lightly Mg-doped p-AlGaN HIL by using MOCVD could be one possibility. But the crystal growth of such p-AlGaN/p-hBN (HET) structure is quite challenging in the LP-MOVPE due to the growth temperature limitation of LP-MOVPE reactor.

The third challenge is to further improve both the crystalline quality of AlN grown on nano-Photonic Holes (nano-PhH) on sapphire substrate for both the enhancement of η_{int} (IQE) as well as for light-extraction-efficiency (η_{lee}) at the same time, as suggested by Eq. (3). After

1
2
3
4
5
6
7
8
9
10
11
12
13
14
15
16
17
18
19
20
21
22
23
24
25
26
27
28
29
30
31
32
33
34
35
36
37
38
39
40
41
42
43
44
45
46
47
48
49
50
51
52
53
54
55
56
57
58
59
60

implementing the optimized AlGaN MQWs structure for optically pumped UV laser, we observed stimulated emission by optical pumping from the AlGaN DUV quantum wells with very low threshold exciting power density of 68 kW/cm^2 at RT. Very recently we also realized electrically pumped ridge UVB laser structure using the optimized MQWs structure in this work, where we successfully enhanced the injected current density from 0.1 kA/cm^2 to 7 kA/cm^2 under pulse-operation in the range of millisecond at RT. However, further improvement of η_{lee} and reduction of total-TDDs in the n-AlGaN EIL underneath the MQWs are expected, by using the specially designed nano-patterned–sapphire substrate (nano-PSS) as well as PhC either in p-AlGaN contact layer of UVB LEDs or in the p-GaN contact layer on the p-AlGaN HIL [40-41]. To verify the effectiveness of nano-PSS for both total-TDDs reduction (η_{int} enhancement in MQWs) and η_{lee} enhancement in the UVB LEDs, we need to investigate different shapes and sizes of nanostructures or patterns. If we compare the nano-PSS with micro-PSS, the optical power is expected to be high in the case of optimized nano-PSS structure for the target emission wavelength of UVB light. AlN template on nano-PSS both for light management and total-TDDs reduction up to 1-2×10^8 cm^{-2} in n-AlGaN EIL underneath the MQWs may be possible to enhance the η_{int} up to 70-80%, as shown in Fig. 10(d) [38-39]. Last but not the least, we need to explore some new p-type dopant materials for p-AlGaN-based UV emitters including LDs [50] to replace the conventional Mg-doped p-type p-AlGaN HIL and p-AlGaN CL.

5. Conclusion

In conclusion, ultimately the issue of nonlinearity in the light output power (L) and external-quantum-efficiency (η_{ext}) were successfully overcome during the operation of 310nm-band UVB LEDs. Subsequently, the η_{ext} up to 4.7% and L up to 29 mW in the 310nm-band UVB LED under pulse-operation on bare-wafer at RT was achieved. Such improvement in the 310nm-band UVB LED is attributed to the optimal distribution of electron-hole inside the MQWs after reduction of quantum-well-barrier (T_{QWB}) for efficient hole transport as well as to the relaxing of n-AlGaN electron-injection-layer (EIL) up to 50% underneath the MQWs. This result of 310nm-band UVB light emission is quite promising for the treatment of cancer, immunotherapy, vulgaris treatment, and growth of plant under UVB-lighting for phytochemical enrichment. For 294nm-band UVB LED, when the Al-contents were increased from 48% to 55% in the undoped (ud)-AlGaN final barrier (FB), and the Al-contents difference between QWBs and QWs of MQWs were also increased from 15% to 20%, the maximum L was greatly enhanced from 17 mW to a record value of 32mW on bare-wafer under pulse-operation at RT. Similarly, the maximum η_{ext} was also improved remarkably from 5.6 % to 6.5 % under both CW and pulse-operation at RT, using Ni (1nm) /Al (200 nm) p-electrode and using new design of moderately Mg-doped p-MQB EBL. This result of 294nm-band UVB light emission is expected to be promising for production of vitamins D_3 in both human body as well as in animal body too. Importantly, such controllable multi UVB-wavelength LED may extend nitride - based LED to previously inaccessible areas, for example, UVB laser and other futuristic devices such as sensors.

Funding. This work was partially supported by the Nippon Tungsten co., LTD, Japan and partially supported by the New Energy and Industrial Technology Development Organization (NEDO), Japan at Quantum Optodevice Laboratory (QOL).

Acknowledgment. The authors would like to thank Dr. Russell Deacon of the RIKEN for fruitful discussion and NEDO Japan for financial support.

Disclosures. The authors declare no conflicts of interest.

1
2
3
4
5
6
7
8
9
10
11
12
13
14
15
16
17
18
19
20
21
22
23
24
25
26
27
28
29
30
31
32
33
34
35
36
37
38
39
40
41
42
43
44
45
46
47
48
49
50
51
52
53
54
55
56
57
58
59
60

References

1. IUVA Press Release (Jan 24, **2020**). IUVA Fact Sheet on UV Disinfection for COVID-19. Retrieved from http://iuva.org/Projects-Articles-Repository/8672736
2. Parrish, J. A.; and Jaenicke, K. F. Action spectrum for phototherapy of psoriasis J. Invest. Dermatol. **1981**, 76, 359-362.
3. Khan, M. A.; Matsuura, E.; Kashima, Y.; and Hirayama, H. Overcoming the current injection issue in the 310 nm band AlGaN UVB light-emitting diode Jpn. J. Appl. Phys. **2020**, 59, SAAD01.
4. Khan, M. A.; Matsuura, E.; Kashima, Y.; and Hirayama, H. Influence of Undoped-AlGaN Final Barrier of MQWs on the Performance of Lateral-Type UVB LEDs Phys. Status Solidi A **2019**, 216, 1900185.
5. Kalajian, T. A.; Aldoukhi, A.; Veronikis, A. J.; Persons, K.; and Holick, M. F. Ultraviolet B Light Emitting Diodes (LEDs) Are More Efficient and Effective in Producing Vitamin D3 in Human Skin Compared to Natural Sunlight Sci. Rep. **2017**, 7, 11489.
6. Lerche, C. M.; Philipsen, P. A.; and Wulf, H. C. UVR: sun, lamps, pigmentation and vitamin D Photochem. Photobiol. Sci. **2017**, 16, 291-301.
7. Hirayama, H.; Maeda, N.; Fujikawa, S.; Toyoda, S.; and Kamata, N. Recent progress and future prospects of AlGaN-based high-efficiency deep-ultraviolet light-emitting diodes Jpn. J. Appl. Phys. **2014**, 53, 100209.
8. Kneissl, M.; and Rass, J. III-Nitride Ultraviolet Emitters-Technology and Applications, Springer Series in Material Science (Springer) **2016**, Vol. 227, Ch. 1.
9. Zhou, C.; Ghods, A.; Saravade, V.; Patel, P.; Yunghans, K.; Ferguson, C.; Feng, Y.; Kucukgok, B.; Lu, N.; and Ferguson, I. Review—The Current and Emerging Applications of the III-Nitrides ECS J. Solid State Sci. Technol. **2017**, 6, Q149-Q156.
10. Matsuura, S.; and Ishikura, S. Suppression of Tomato mosaic virus disease in tomato plants by deep ultraviolet irradiation using light-emitting diodes Letters in Applied Microbiology **2014**, 59, 457-463.
11. Ramnemark, A.; Norberg, M.; Pettersson-Kymmer, U.; Eliasson M. Adequate vitamin D levels in a Swedish population living above latitude 63°N: The 2009 Northern Sweden MONICA study Int J Circumpolar Health **2015**, 74, 27963.
12. Insel, Paul M.; Elaine Turner, R.; Ross, D. **2004** Nutrition. 2nd Pkg edition, Jones & Bartlett Publishing, ISBN-10: 0763747289.
13. Wollina, U., Unger, L.; Heinig, B; Kittner, T. Psoroatic arthritis. Dermatol. Ther. **2010**, 23, 123–136.
14. Nast, A.; Boehncke, W. H.; Mrowietz, U; Ockenfels, H. M.; Philipp, S.; Reich, K.; Rosenbach, T.; Sammain, A.; Schlaeger, M.; Sebastian, M.; Sterry, W.; Streit, V.; Augustin, M.; Erdmann, R.; Klaus, J.; Koza, J.; Muller , S.; Orzechowski, H. D.; Rosumeck, S.; Schmid-Ott, G.; Weberschock, T.; Rzany, B. S3 - Guidelines on the treatment of psoriasis vulgaris (English version) J. Dtsch. Dermatol. Ges. **2012**, 10 (Suppl 2), S1–95.
15. Verhaeghe, E.; Lodewick, E.; van Geel, N.; Lambert, J. Intrapatient Comparison of 308-nm Monochromatic Excimer Light and Localized Narrow-Band UVB Phototherapy in the Treatment of Vitiligo: A Randomized Controlled Trial Dermatology **2011**, 223, 343–348.
16. Morison, W. L. Phototherapy and Photochemotherapy of Skin Disease. 2nd edn, **1991** Raven Press, New York.
17. Hockberger, P. E. A History of Ultraviolet Photobiology for Humans, Animals and Microorganisms Photochem. Photobiol. **2002**, 76, 561–579.
18. William, D. J. Clinical Dermatology. Saunders Elsevier **2006**, ISBN 0-7216-2921-0 p-335.
19. Torii, K.; Morita, A. UVB irradiation induces HMGB1 expression in keratinocytes without promoting apoptosis Exp Dermatol. **2016**, 25, 741-742.
20. Kemény, L.; Csoma, Z.; Bagdi, E.; Banham, A. H.; Krenács, L.; Koreck, A. Targeted phototherapy of plaque-type psoriasis using ultraviolet B-light-emitting diodes Br. J. Dermatol. **2010**, 163, 167–173.
21. Beani, J. C.; Jeanmougin, M. Narrow-band UVB therapy in psoriasis vulgaris: good practice guideline and recommendations of the French Society of Photodermatology Ann. Dermatol. Venereol. **2010**, 137, 21–31.
22. Ibbotson, S. H.; Bilsland, D.; Cox, N. H.; Dawe, R. S.; Diffey, B.; Edwards, C.; Farr, P. M.; Ferguson, J.; Hart, G.; Hawk, J.; Lloyd, J.; Martin, C.; Moseley, H., McKenna, K.; Rhodes, L. E.; Taylor, D. K. An update

and guidance on narrowband ultraviolet B phototherapy: a British Photodermatology Group Workshop Report Br. J. Dermatol. **2004**, 151, 283–297.

23. Manasevit, H. M.; Erdmann, F. M.; and Simpson, W. I. The Use of Metalorganics in the Preparation of Semiconductor Materials: IV. The Nitrides of Aluminum and Gallium J. Electrochem. Soc. **1971**, 118, 1864.

24. Khan, M. A.; Matsumoto, T.; Maeda, N.; Kamata, N.; and Hirayama, H. Improved external quantum efficiency of 293 nm AlGaN UVB LED grown on an AlN template Jpn. J. Appl. Phys. **2019**, 58, SAAF0120.

25. Khan, M. A.; Maeda, N.; Masafumi, J.; Akamatsu, Y.; Tanabe, R.; Yamada, Y.; and Hirayama, H. 13 mW operation of a 295–310 nm AlGaN UV-B LED with a p-AlGaN transparent contact layer for real world applications J. Mater. Chem. C **2019**, 7, 143-152.

26. Matsumoto, T.; Khan, M. A.; Maeda, N.; Fujikawa, S.; Kamata, N.; and Hirayama, H. Milliwatt power UV-A LEDs developed by using n-AlGaN superlattice buffer layers grown on AlN templates J. Phys. D: Appl. Phys. **2019**, 52, 115102.

27. Kim, K. H.; Fan, Z. Y.; Khizar, M.; Nakarmi, M. L.; Lin, J. Y.; Jiang, H. X. AlGaN-based ultraviolet light-emitting diodes grown on AlN epilayers Appl. Phys. Lett. **2004**, 85, 4777- 4779.

28. Susilo, N.; Enslin, J.; Sulmoni, L.; Guttmann, M.; Zeimer, U.; Wernicke, T., Weyers, M.; Kneissl, M.; Effect of the GaN:Mg Contact Layer on the Light-Output and Current-Voltage Characteristic of UVB LEDs Phys. Status Solidi A **2017**, 215, 1700643.

29. Enslin, J. Metamorphic $Al_{0.5}Ga_{0.5}N$:Si on AlN/sapphire for the growth of UVB LEDs J. Cryst. Growth **2016**, 464, 185-189.

30. Rass, J. High-power UV-B LEDs with long lifetime Proc. SPIE **2015**, 9363, Gallium Nitride Materials and Devices X 93631K.

31. Guttmann, M. Improved light extraction and quantum efficiencies for UVB LEDs with UV-transparent p-AlGaN superlattices (Conference Presentation) Proc. SPIE **2017**, 10104, Gallium Nitride Materials and Devices XII 101041S.

32. Hirayama, H.; Yatabe, T.; Noguchi, N.; Ohashi, T.; and Kamata, N. 231–261nm AlGaN deep-ultraviolet light-emitting diodes fabricated on AlN multilayer buffers grown by ammonia pulse-flow method on sapphire Appl. Phys. Lett. **2007**, 91, 071901.

33. Jo, M.; Maeda, N.; and Hirayama, H. Enhanced light extraction in 260 nm light-emitting diode with a highly transparent p-AlGaN layer Appl. Phys. Express **2016**, 9, 012102.

34. Bernardini, F.; Fiorentini, V. Macroscopic polarization and band offsets at nitride heterojunctions Phys. Rev. B **1998**, 57, R9427.

35. Kohno, T.; Sudo, Y.; Yamauchi, M.; Mitsui, K.; Kudo, H.; Okagawa, H.; and Yamada, Y. Internal Quantum Efficiency and Nonradiative Recombination Rate in InGaN-Based Near-Ultraviolet Light-Emitting Diodes Jpn. J. Appl. Phys. **2012**, 51, 072102.

36. Maeda, N.; Yun, J.; Jo, M.; and Hirayama, H. Enhancing the light-extraction efficiency of AlGaN deep-ultraviolet light-emitting diodes using highly reflective Ni/Mg and Rh as p-type electrodes Jpn. J. Appl. Phys. **2018**, 57, 04FH08.

37. Maeda, N.; Jo, M.; and Hirayama, H. Improving the Light-Extraction Efficiency of AlGaN DUV-LEDs by Using a Superlattice Hole Spreading Layer and an Al Reflector Phys. Status Solidi A **2018**, 215, 1700436.

38. Shatalov, M.; Sun, W.; Bilenko, Y.; Sattu, A.; Hu, X.; Deng, J.; Yang, J.; Shur, M.; Moe, C.; Wraback, M.; and Gaska, R. Large Chip High Power Deep Ultraviolet Light-Emitting Diodes Appl. Phys. Express **2010**, 3, 062101.

39. Ban, K.; Yamamoto, J.; Takeda, K.; Ide, K.; Iwaya, M.; Takeuchi, T.; Kamiyama, S.; Akasaki, I.; and Amano, H. Internal quantum efficiency of whole-composition-range AlGaN multiquantum wells Appl. Phys. Express **2011**, 4, 052101.

40. Kashima, Y. et al. High external quantum efficiency (10%) AlGaN based deep-ultraviolet light-emitting diodes achieved by using highly reflective photonic crystal on p-AlGaN contact layer, Appl. Phys. Express, **2018**, 11 , 012101.

41. Takano, T. et al. Deep-ultraviolet light-emitting diodes with external quantum efficiency higher than 20% at 275 nm achieved by improving light-extraction efficiency, Appl. Phys. Express, **2017**, 10 , 031002.

1
2
3
4
5
6
7
8
9
10
11
12
13
14
15
16
17
18
19
20
21
22
23
24
25
26
27
28
29
30
31
32
33
34
35
36
37
38
39
40
41
42
43
44
45
46
47
48
49
50
51
52
53
54
55
56
57
58
59
60

42. Dalmau, R.; and Moody, B. (Invited) Polarization-Induced Doping in Graded AlGaN Epilayers Grown on AlN Single Crystal Substrates ECS Transactions **2018**, 86, 31-40.

43. Adhikari, J.; and Kofke, D. A. Molecular simulation study of miscibility in $In_xGa_{1-x}N$ ternary alloys J. Appl. Phys. **2004**, 95, 4500.

44. Ho. H.; and Springfellow, G. B. Incomplete solubility in nitride alloys. In: III-V Nitrides, MRS Proc.**1997**, 449, 871–880.

45. Cremades, A.; Albrecht, M.; Krinke, J.; Dimitrov, R.; Stutzmann, M. Effects of phase separation and decomposition on the minority carrier diffusion length in $Al_xGa_{1-x}N$ films J. Appl. Phys. **2000**, 87, 2357.

46. Marques, M.; Teles, L. K.; and Ferreira, L. G. Influence of miscibility on the energy-gap dispersion in $Al_xGa_{1-x}N$ alloys: First-principles calculations Phys. Rev. B **2007**, 75, 033201.

47. Bryan, I.; Bryan, Z.; Mita, S.; Rice, A.; Hussey, L.; Shelton, C.; Tweedie, J.; Maria, J. P.; Collazo, R.; Sitart, Z. The role of surface kinetics on composition and quality of AlGaN J. Cryst. Growth **2016**, 451, 65.

48. Zeimer, U.; Kueller, V.; Knauer, A.; Mogilatenko, a.; Weyers, M.; and Kneissl, M. High quality AlGaN grown on ELO AlN/sapphire templates J. Cryst. Growth **2013**, **377**, 32.

49. Khan, M. A.; Takeda, R.; Yamada, y.; Maeda, N.; Jo, M.; and Hirayama, H. Beyond 53% internal quantum efficiency in a AlGaN quantum well at 326 nm UVA emission and single-peak operation of UVA LED Opt. Lett. **2020**, 45, 495-498.

50. Hirayama, H.; Maeda, N.; Jo, M.; Khan, M. A.; Tadatomo, K.; Okada, N.; and Yamada, Y. Recent Progress toward realizing AlGaN-based Deep-UV Laser Diodes. The Review of Laser Engineering **2019**, 47, 196.

51. Liu, J. P.; Ryou, J. H.; Dupuis, R. D.; Han, J.; Shen, G. D.; and Wang, H. B. Barrier effect on hole transport and carrier distribution in InGaN/GaN multiple quantum well visible light-emitting diodes Appl. Phys. Lett. **2008**, 93, 021102.

52. Tamulaitis, G. in "Handbook of Solid-State Lighting and LEDs", edited by Zhe Chuan Feng, CRC Press Taylor & Francis Group 6000 Broken Sound Parkway NW, **2017**, Section-III, chapter 11.

53. Ferdinand Scholz, in Compound Semiconductors: Physics, Technology, and Device 18 Concepts. (Ed: F. Scholz) Pan Stanford, Singapore **2018**, Ch. 11.

54. Hirayama, H.; and Khan, M. A. Keynote- Problems and latest achievements in AlGaN-based deep-UV LEDs presented in the IWUMD-4, September 8-13, **2019**, Saint Petersburg, Russia.

55. Rimini, E., in "Surface modification and alloying by laser, ion and electron beams", edited by Poate, J. M.; Foti, G.; and Jacobsen, D. Plenum press, (New York), **1983**, Ch. 2 p.26.

56. Bermundo. J. P. S.; Ishikawa, Y.; Fujii, M. N.; Ikenoue, H.; Uraoka, Y. Instantaneous Semiconductor-to-Conductor Transformation of a Transparent Oxide Semiconductor a-InGaZnO at 45 °C ACS Appl. Mater. Interfaces **2018**, 10, 24590.

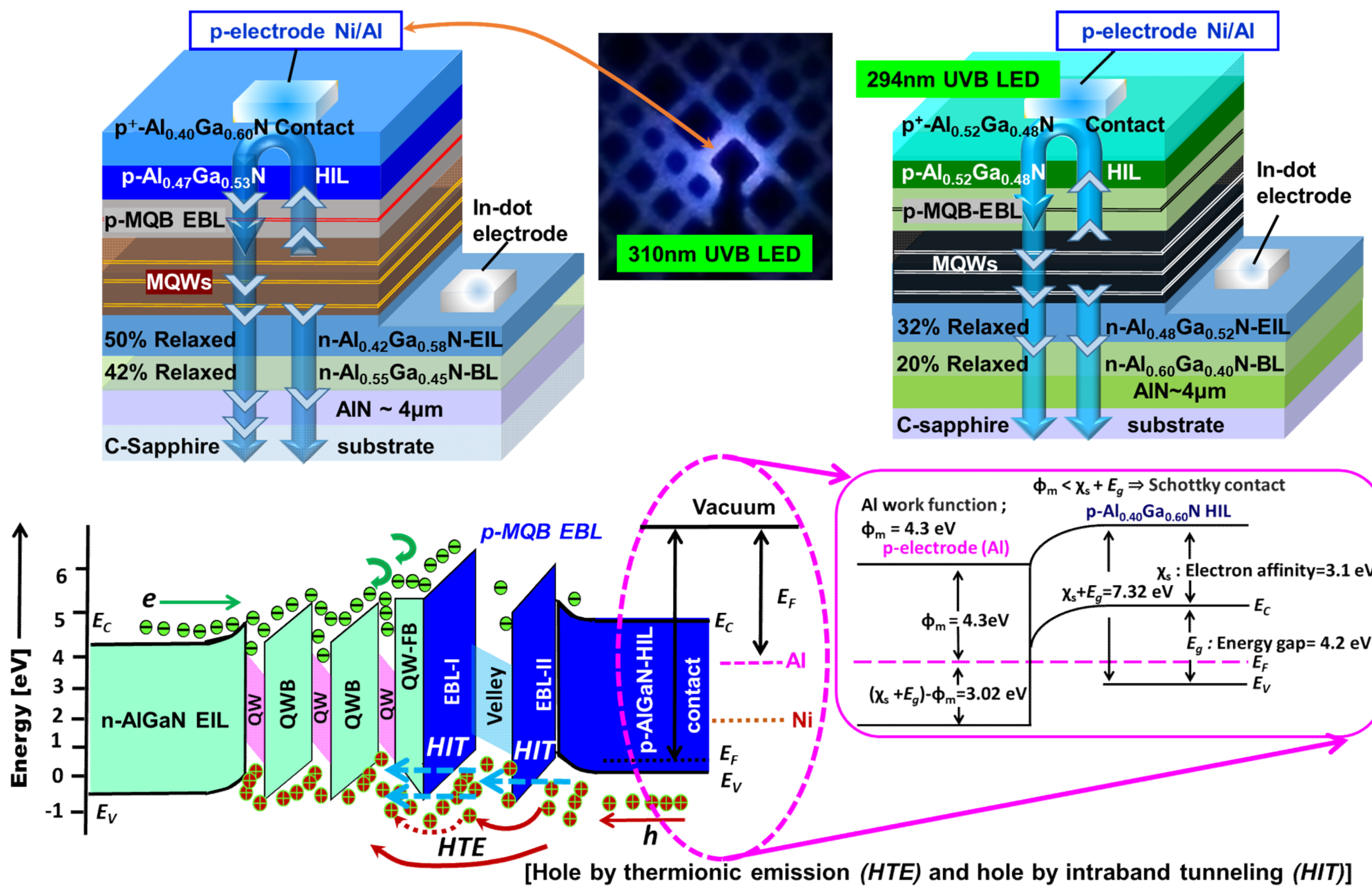
p-electrode Ni/Al
p+-Al0.40Ga0.60N Contact
p-Al0.47Ga0.53N HIL
p-MQB EBL
MQWs
50% Relaxed n-Al0.42Ga0.58N-EIL
42% Relaxed n-Al0.55Ga0.45N-BL
AlN ~ 4μm
C-Sapphire substrate
In-dot electrode
310nm UVB LED
p-electrode Ni/Al
294nm UVB LED
p+-Al0.52Ga0.48N Contact
p-Al0.52Ga0.48N HIL
p-MQB-EBL
MQWs
In-dot electrode
32% Relaxed n-Al0.48Ga0.52N-EIL
20% Relaxed n-Al0.60Ga0.40N-BL
AlN~4μm
C-sapphire substrate
Energy [eV]
e
h
HTE
HIT
p-MQB EBL
n-AlGaN EIL
QW
QWB
QW-FB
EBL-I
Velley
EBL-II
p-AlGaN-HIL
contact
Vacuum
Al
Ni
Al work function ;
ϕm = 4.3 eV
p-electrode (Al)
ϕm < χs + Eg ⇒ Schottky contact
p-Al0.40Ga0.60N HIL
χs : Electron affinity=3.1 eV
χs+Eg=7.32 eV
ϕm = 4.3eV
Eg : Energy gap= 4.2 eV
(χs +Eg)-ϕm=3.02 eV
[Hole by thermionic emission (HTE) and hole by intraband tunneling (HIT)]